Competitive binding

Competitive binding assays were performed in the presence of GST-fused wild-type ERRγ-LBD or its mutants at the most appropriate concentration of each. Reaction mixtures were incubated with [^{3}H]BPA (5 nM in final) at 4 °C overnight, and free radioligand was removed by the method described above after incubation with 100 μL of 1% dextran-coated charcoal in NaCl/P_i (pH 7.4) for 10 min at 4 °C. To estimate the binding affinity, the IC_{50} values were calculated from the dose–response curves evaluated by the nonlinear analysis program ALLFIT [27]. Each assay was performed in duplicate and repeated at least three times.

Cell culture and transient transfection assays

HeLa cells were maintained in Eagle's modified Eagle medium (EMEM) (Nissui, Tokyo, Japan) in the presence of 10% (v/v) fetal bovine serum at 37 °C. HeLa cells were seeded at 5×10^5 cells/dish (6 cm in diameter) for 24 h and then transfected with a mixture of 3 μg of luciferase reporter gene (pGL3/3xERRE), 1 μg of the expression plasmid of wild-type ERRγ or its mutant [pcDNA3.1(+)/ERRγ-WT or mutations] and, as an internal control, 10 ng of pSEAP-control plasmid by Plus reagent (10 μL·mL^{-1}; Invitrogen) and Lipofectamine (15 μL·mL^{-1}), according to the manufacturer's protocol. Approximately 24 h after transfection, cells were harvested and plated into 96-well plates at a concentration of 5×10^4 cells/well. The cells were then treated with varying doses of chemicals diluted with 1% BSA/NaCl/P_i (v/v).

After 24 h, luciferase activity was measured by using Luciferase assay reagent (Promega, Madison, WI, USA) according to the manufacturer's instructions. SEAP activity was assayed by using Great EscAPe™ SEAP assay reagent (Clontech Laboratories) according to the Fluorescent SEAP Assay protocol. Light emission was measured on a microplate reader Wallac 1420 ARVOsx (Perkin Elmer, Turku, Finland). Cells treated with 1% BSA/NaCl/P_i were used as a vehicle control. Values were computed as fold inductions after normalization to SEAP activities. Each assay was performed in duplicate and repeated at least three times.

Acknowledgements

We thank Professor Ian A. Meinertzhagen, Dalhousie University, Canada, for reading the manuscript. This study was supported in part by Health and Labour Sciences Research Grants for Research on Risk of Chemical Substances from the Ministry of Health, Labor and Welfare of Japan. This work was also supported in part by grants-in-aid from the Ministry of Education, Science, Sports and Culture in Japan to YS.

References

1 Dodds EC & Lawson W (1938) Molecular structure in relation to oestrogenic activity. Compounds without a phenanthrene nucleus. *Proc R Soc Lond B Biol Sci* **125**, 222–232.
2 Krishnan AV, Stathis P, Permuth SF, Tokes L & Feldman D (1993) Bisphenol-A: an estrogenic substance is released from polycarbonate flasks during autoclaving. *Endocrinology* **132**, 2279–2286.
3 Olea N, Pulgar R, Perez P, Olea-Serrano F, Rivas A, Novillo-Fertrell A, Pedraza V, Soto AM & Sonnenschein C (1996) Estrogenicity of resin-based composites and sealants used in dentistry. *Environ Health Perspect* **104**, 298–305.
4 Sohoni P & Sumpter JP (1998) Several environmental oestrogens are also anti-androgens. *J Endocrinol* **158**, 327–339.
5 Xu LC, Sun H, Chen JF, Bian Q, Qian J, Song L & Wang XR (2005) Evaluation of androgen receptor transcriptional activities of bisphenol A, octylphenol and nonylphenol in vitro. *Toxicology* **216**, 197–203.
6 vom Saal FS, Cooke PS, Buchanan DL, Palanza P, Thayer KA, Nagel SC, Parmigiani S & Welshons WV (1998) A physiologically based approach to the study of bisphenol A and other estrogenic chemicals on the size of reproductive organs, daily sperm production, and behavior. *Toxicol Ind Health* **14**, 239–260.
7 Kubo K, Arai O, Omura M, Watanabe R, Ogata R & Aou S (2003) Low dose effects of bisphenol A on sexual differentiation of the brain and behavior in rats. *Neurosci Res* **45**, 345–356.
8 vom Saal FS & Hughes C (2005) An extensive new literature concerning low-dose effects of bisphenol A shows the need for a new risk assessment. *Environ Health Perspect* **113**, 926–933.
9 National Toxicology Program (NTP) (2001) US Department of Health and Human Services, National Institute of Environmental Health Sciences, National Toxicology Program's Report of the Endocrine Disruptors Low-Dose Peer Review. Available at http://ntp-server.inehs.nih.gov./htdcs/liason/LowDoseWebPage.html.
10 Safe SH, Pallaroni L, Yoon K, Gaido K, Ross S & McDonnell D (2002) Problems for risk assessment of endocrine-active estrogenic compounds. *Environ Health Perspect* **110**, 925–929.
11 Gray GM, Cohen JT, Cunha G, Hughes C, McConnell EE, Rhomberg L, Sipes IG & Mattison D (2004) Weight of the evidence evaluation of low dose reproductive and developmental effects of bisphenol A. *Hum Ecol Risk Assess* **10**, 875–921.
12 Takayanagi S, Tokunaga T, Liu X, Okada H, Matsushima A & Shimohigashi Y (2006) Endocrine disruptor bisphenol A strongly binds to human estrogen-related

receptor γ (ERRγ) with high constitutive activity. *Toxicol Lett* **167**, 95–105.
13 Robinson-Rechavi M, Carpentier AS, Duffraisse M & Laudet V (2001) How many nuclear hormone receptors are there in the human genome? *Trends Genet* **17**, 554–556.
14 Giguere V (2002) To ERR in the estrogen pathway. *Trends Endocrinol Metab* **13**, 220–225.
15 Horard B & Vanacker JM (2003) Estrogen receptor-related receptors: orphan receptors desperately seeking a ligand. *J Mol Endocrinol* **31**, 349–357.
16 Eudy JD, Yao S, Weston MD, Ma-Edmonds M, Talmadge CB, Cheng JJ, Kimberling WJ & Sumegi J (1998) Isolation of a gene encoding a novel member of the nuclear receptor superfamily from the critical region of Usher syndrome type IIa at 1q41. *Genomics* **50**, 382–384.
17 Hong H, Yang L & Stallcup MR (1999) Hormone-independent transcriptional activation and coactivator binding by novel orphan nuclear receptor ERR3. *J Biol Chem* **274**, 22618–22626.
18 Heard DJ, Norby PL, Holloway J & Vissing H (2000) Human ERRgamma, a third member of the estrogen receptor-related receptor (ERR) subfamily of orphan nuclear receptors: tissue-specific isoforms are expressed during development and in the adult. *Mol Endocrinol* **14**, 382–392.
19 Greschik H, Wurtz JM, Sanglier S, Bourguet W, van Dorsselaer A, Moras D & Renaud JP (2002) Structural and functional evidence for ligand-independent transcriptional 1 evidence for ligand-independent transcriptional activation by the estrogen-related receptor 3. *Mol Cell* **9**, 303–313.
20 Matsushima A, Kakuta Y, Teramoto T, Koshiba T, Liu X, Okada H, Tokunaga T, Kawabata S, Kimura M & Shimohigashi Y (2007) Structural evidence for endocrine disruptor bisphenol A binding to human nuclear receptor ERRγ. *J Biochem* **142**, 517–524.
21 Nelson RM & Long GL (1989) A general method of site-specific mutagenesis using a modification of the *Thermus aquaticus* polymerase chain reaction. *Anal Biochem* **180**, 47–51.
22 Greschik H, Flaig R, Renaud JP & Moras D (2004) Structural basis for the deactivation of the estrogen-related receptor gamma by diethylstilbestrol or 4-hydroxytamoxifen and determinants of selectivity. *J Biol Chem* **279**, 33639–33646.
23 Sambrook J & Russell DW (2001) *Molecular Cloning: A Laboratory Manual*, 3rd edn. Cold Springs Harbor Laboratory Press, Cold Spring Harbor, NY.
24 Coward P, Lee D, Hull MV & Lehmann JM (2001) 4-Hydroxytamoxifen binds to and deactivates the estrogen-related receptor gamma. *Proc Natl Acad Sci USA* **98**, 8880–8884.
25 Bradford MM (1976) A rapid and sensitive method for the quantitation of microgram quantities of protein utilizing the principle of protein-dye binding. *Anal Biochem* **72**, 248–254.
26 Nakai M, Tabira Y, Asai D, Yakabe Y, Shimyozu T, Noguchi M, Takatsuki M & Shimohigashi Y (1999) Binding characteristics of dialkyl phthalates for the estrogen receptor. *Biochem Biophys Res Commun* **254**, 311–314.
27 DeLean A, Munson PJ & Rodbard D (1978) Simultaneous analysis of families of sigmoidal curves: application to bioassay, radioligand assay, and physiological dose–response curves. *Am J Physiol* **235**, E97–E102.

J. Biochem. **141,** 867–877 (2007)
doi:10.1093/jb/mvm094

Double-labelled *in situ* Hybridization Reveals the Lack of Co-localization of mRNAs for the Circadian Neuropeptide PDF and FMRFamide in Brains of the Flies *Musca domestica* and *Drosophila melanogaster*

Ayami Matsushima[1], Katsuhiro Takano[2], Taichi Yoshida[1], Yukimasa Takeda[1], Satoru Yokotani[1], Yasuyuki Shimohigashi[1,*] and Miki Shimohigashi[2]

[1]Laboratory of Structure-Function Biochemistry, Department of Chemistry, Faculty and Graduate School of Sciences, Kyushu University, Fukuoka 812-8581, Japan; and [2]Division of Biology, Faculty of Science, Fukuoka University, Fukuoka 814-0180, Japan

Received January 9, 2007; accepted March 31, 2007; published online April 10, 2007

Many lines of evidence have suggested that neuropeptides other than pigment-dispersing factor (PDF) are involved in regulating insect circadian rhythms, and FMRFamide-related peptides are additional candidates acting as such neuromodulators. Double-immunolabelling in insect brains with anti-crustacean β-PDH and anti-FMRFamide antibodies had previously suggested that insect PDF and FMRFamide-like peptides may coexist in the same cells. However, it is critical for this kind of comparative investigations to use antibodies of proven specificity, to eliminate the possibility of both reciprocal cross-reactivity and the detection of unknown peptides. In the present study, we achieved the cDNA cloning of an *fmrf* mRNA from the housefly *Musca domestica*, for which co-localization of FMRFamide and PDF peptides was previously suggested. In order to examine the possible co-expression of this gene with the *pdf* gene, we carried out double-labelled *in situ* hybridization for simultaneous detection of both *pdf* and *fmrf* mRNAs in housefly, *Musca* brains. The results clearly indicated that they occur in distinctly different cells. This was also proven for the fruit fly *Drosophila melanogaster* by similar double-labelled *in situ* hybridization. The results thus revealed no reason to evoke the physiological release of FMRFamide and PDF peptides from the same neurons.

Key words: circadian rhythm, double-labelled *in situ* hybridization, FMRFamides, neuropeptides, pigment-dispersing factor (PDF).

Abbreviations: AAP, Abridged Anchor Primer; AP, alkaline phosphatase; AUAP, Abridged Universal Anchor Primer; BCIP, 5-bromo-4-chloro-3-indolylphosphate; DCV, dense core vesicle; DIG, digoxigenin; FaRPs, FMRFamide-related peptides; FITC, fluorescein isothiocyanate; FMRFamide, the one-letter amino acid code denotes H–Phe–Met–Arg–Phe–NH_2; HRP, horseradish peroxidase; NBT, 4-nitro-blue tetrazolium chloride; NTMT, a solution containing 100 mM NaCl, 100 mM Tris–HCl (pH 9.5), 50 mM MgCl2 and 1% Tween 20; PBS, phosphate buffered saline; PBST, PBS containing 0.1% Tween 20; PDF, pigment-dispersing factor; PDH, pigment-dispersing hormone; RACE, rapid amplification of cDNA ends; RT-PCR, reverse transcription PCR; TBS, Tris-buffered saline; TBST, TBS containing 1% Tween 20.

FMRFamide (H–Phe–Met–Arg–Phe–NH_2) is a neuropeptide originally isolated from the mollusk *Macrocallista nimbosa* and identified by monitoring its cardioexcitatory activity on the clam heart (*1*). Peptides containing C-terminal FMRFamide or a related sequence are members of a large family of structurally related peptides found in both invertebrate and vertebrate species. In insects, these peptides are called FMRFamide-related peptides (FaRPs) and three major families have been reported to date, including FMRFamides, sulfakinins (*2*) and myosuppressins (*3, 4*). However, little is known about their physiological functions.

Another insect amide peptide, pigment-dispersing factor (PDF), was first found in brains of the grasshopper and its melanophore pigment-dispersing activity monitored in crabs (*5*). Insect PDF is composed of 18 amino acids and involved in the regulation of circadian rhythms as an output neuromodulator (*6–14*). Its involvement in circadian rhythm was shown by the mutant fruit fly *Drosophila melanogaster* designated pdf^{01}. pdf^{01} was found to have a nonsense mutation at the residue 21 of prepro-PDF, converting a Tyr (TA*C*) to a stop codon (TA*A*). This mutant shows abnormal behaviour, the evening activity peak being advanced by approximately 1 h (*11*). The result revealed the substantial importance of *pdf* in circadian system. In order to elucidate the molecular mechanism of PDF peptide in the regulation of circadian rhythms, we have cloned *pdf*

*To whom correspondence should be addressed. Tel/Fax: +81-92-642-2584, E-mail: shimoscc@mbox.nc.kyushu-u.ac.jp

The nucleotide sequence datum reported in this article has been submitted to the DDB/EMBL/GenBank Data libraries under accession number AB214648.

mRNAs from several insects and clarified the existence of four different types of precursor proteins (*15–19*).

In recent years, there have also been several reports suggesting the involvement of neuropeptides other than PDF in the circadian regulatory system, and FMRFamide peptides have been proposed as candidates for such neuromodulators. Microinjection of FMRFamide peptides into the brains of houseflies, for example, confirmed a strong interrelation between this neuropeptide and circadian rhythms in the visual system (*20*). Double-immunolabelling in insect brains using anti-crustacean β-PDH and anti-FMRFamide antibody had suggested moreover that insect PDF and FMRFamide-like peptides may co-exist in the same cells in several different insect species (*20–23*). However, immunocytochemical investigations crucially require the use of highly specific antibodies against each peptide in order to avoid possible cross-reactivity to unknown peptides.

As a check, multiple-labelling *in situ* hybridization techniques can provide sensitive cytochemical information about more than two different mRNA genes in the same preparation. This method requires the precise nucleotide sequence of a target mRNA in the preparation of cRNA probes. The recent cDNA cloning and *in situ* hybridization of *pdf* mRNA of the house fly *Musca domestica* (*17*), provided an excellent opportunity to examine the co-localization of *pdf* with *fmrf* mRNA in the *Musca* brain. *Musca* has a brain size bigger than that of the fruit fly *Drosophila* and this is definitely advantageous to identify the mRNA-expressing cells as a prior experiment to the analysis for *Drosophila* brain. Thus, in the present study we first carried out molecular cloning of *Musca fmrf* mRNA.

For insect FMRFamide-related peptides, available cloning data have hitherto been limited to two different fruit fly species, *D. melanogaster* and *D. virilis*. The *D. melanogaster fmrf* gene was identified by screening the genomic library using *fmrf* cDNA sequence data from the marine mollusk *Aplysia californica* (*24*) and eventually found to encode 13 copies of 8 different FaRPs, five copies of which are exactly identical (*25*). The *fmrf* gene of *D. virilis* was also cloned by screening the genomic library using the *D. melanogaster* genome fragment lying 5′ upstream of the *fmrf* mRNA start site (*26*). This *fmrf* gene encodes 10 different FaRPs, six of which are different from *D. melanogaster* FaRPs. Although such a low sequence similarity makes the search for *fmrf* genes in insects very difficult, based on this sequence information we planned to clone the housefly *fmrf* gene. Here we describe the results of cDNA cloning of the *Musca fmrf* gene and double-labelled *in situ* hybridization of both *fmrf* and *pdf* mRNAs.

MATERIALS AND METHODS

Animals—The housefly *Musca domestica* was purchased from Sumika Technoservice Co. (Takarazuka). All flies were maintained at 25°C under a day:night cycle of L12:D12. To collect brain samples for cDNA cloning, the flies were dissected under a microscope and their brains were immediately frozen in liquid nitrogen. Dissected thoracic ganglia of males and females were stored at −80°C until use. For *in situ* hybridization, 5-day-old female houseflies were used.

3′ RACE for Identification of 3′ End Coding Musca fmrf cDNA—The cDNA cloning of the *Musca fmrf* gene was carried out by the 3′ RACE method (*27*). mRNAs were extracted from the thoracic ganglia dissected from about 30 flies using a QuickPrep® *Micro* mRNA Purification Kit (Amersham Biosciences, Piscataway, NJ, USA) according to the Manufacturer's instructions. The mRNAs (300 ng) were reverse-transcribed by Super Script™ II reverse transcriptase (Invitrogen, Carlsbad, CA, USA) using $d(T)_{17}$-adapter primer (5′-GGCCACGCGTCGACTAGTAC-T_{17}-3′) at 42°C, as previously described (*16*). The resulting cDNAs were subjected to the polymerase chain reaction (PCR) using adaptor primer (5′-GGCCACGCGTCGACTAGTAC-3′) and degenerated primers PKQDFMRFG-F (5′-CCIHVI CARGAYTTYATGMGITT-3′), QDFMRFGR-F (5′-CARG AYTTYATGMGITTYGGIMG-3′) or DNFMRFGR-F (5′-GAYAAYTTYATGMGITTYGGIMG-3′). In these primers, the letters H, V, M, R and Y denote the nucleotides (not G), (not T), (A or C), (A or G) and (C or T), respectively. The primer was designed based on amino acid sequence homology between the FaRP peptide sequences for *D. melanogaster* and *Calliphora vomitoria* (*28*). PCR was performed using AccuPrime™ *Taq* DNA polymerase (Invitrogen) with a slight modification for touch-down PCR condition (*29*): *i.e.* the reaction condition used, 3 min at 94°C followed by 3 cycles of 94°C for 30 s, 68°C for 30 s, 72°C for 60 s, 3 cycles of 94°C for 30 s, 65°C for 30 s, 72°C for 60 s, 3 cycles of 94°C for 30 s, 63°C for 30 s, 72°C for 60 s, 3 cycles of 94°C for 30 s, 60°C for 30 s, 72°C for 60 s, 3 cycles of 94°C for 30 s, 58°C for 30 s, 72°C for 60 s, 25 cycles of 94°C for 30 s, 56°C for 30 s, 72°C for 60 s and a final extension for 7 min at 72°C. The PCR products were subcloned into pBluescript II SK+ and the sequence was analysed by a Thermo Sequenase Cy5.5 dye terminator cycle sequencing kit (Amersham Biosciences).

On the basis of the *Musca fmrf* sequence so obtained, gene-specific primers were newly designed and 3′ RACE was performed for a second time. The primers used were MuscaFMRF-F1 (5′-TGGCCGTAGTCCAGGAAGCCAA-3′ corresponding to the nucleotide sequence 1008–1029 in Fig. 1) and MuscaFMRF-F2 (5′-GCATCGGGTGGACA AGACTTCAT-3′ corresponding to the nucleotide sequence 1159–1181 in Fig. 1). The sequence analysed was confirmed by sequencing several other clones simultaneously.

5′ RACE for Identification of 5′ End Encoding Musca fmrf cDNA—To amplify the 5′ end of the *M. domestica fmrf* (denoted hereafter as *Musca fmrf*) cDNA, 5′ RACE (*26*) using the 5′ RACE System for Rapid amplification of cDNA ends Version 2.0 (Invitrogen) was performed according to the Manufacturer's protocol with some modifications. First-strand cDNA was synthesized from an mRNA by Super Script™ II reverse transcriptase (Invitrogen) with a *Musca fmrf*-specific antisense primer MuscaFMRF-R3 (5′-AAGCTCATGTTTATCGAAT-3′, corresponding to the nucleotide sequence 1485–1503 in Fig. 1) at 42°C. The product was digested by RNase H/T_1 to remove the original mRNA template.

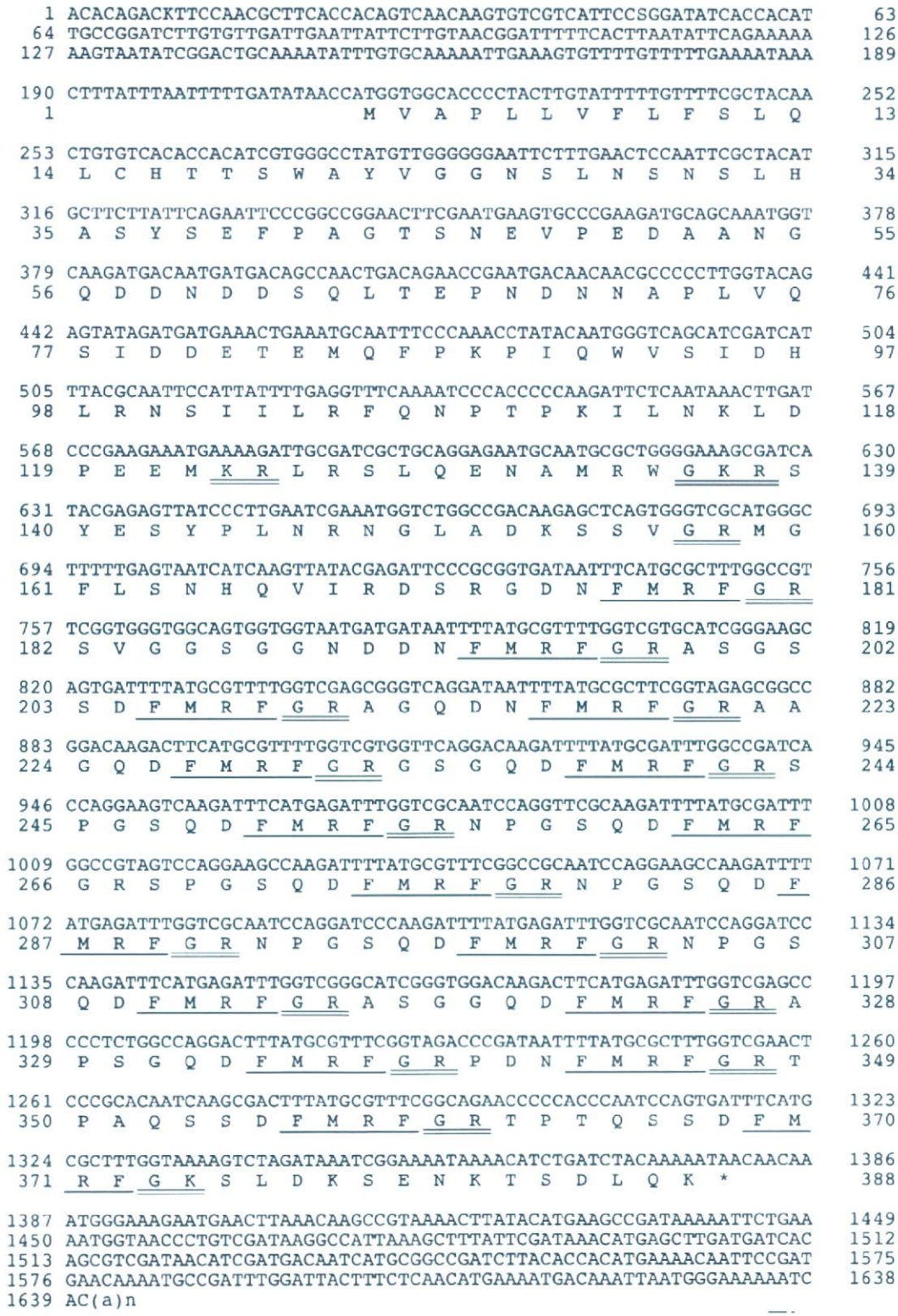

Fig. 1. **Nucleotide and deduced amino acid sequences of *Musca* FMRFamide.** A full-length cDNA clone comprises 1640 bp encoding a precursor protein of 388 amino acid residues. The FMRF structures, Phe–Met–Arg–Phe, are underlined, and the dibasic KR sites and monobasic sites GR and GK are double-underlined.

A homopolymeric tail poly(C) was elongated by using terminal deoxynucleotidyl transferase and a substrate dCTP. The resulting tailed cDNA was amplified by the Abridged Anchor Primer AAP (5′-GGCCACGCGTCG ACTAGTACGGGIIGGGIIGGGIIG-3′ provided by the kit, Life Tech.) and a *Musca fmrf* gene-specific antisense primer MuscaFMRF-R2 (5′-GGCCTTATCGACAGGGT TACCATTT-3′, corresponding to the nucleotide sequence 1449–1473 in Fig. 1) under the conditions essentially as for 3′ RACE. The PCR product was further amplified with Abridged Universal Anchor Primer (AUAP) (5′-GGC CACGCGTCGACTAGTAC-3′, Invitrogen) and *Musca fmrf* gene-specific antisense nested primer MuscaFM RF-R1 (5′-CTTCATGTATAAGTTTTACGGCTTGTT-3′ corresponding to the nucleotide sequence 1406–1432 in Fig. 1). The respective PCR and sequence analyses were carried out as described earlier, and the sequence analysed was confirmed by sequencing several different clones simultaneously.

In order to obtain the authentic full-length 5′ end, further 5′ RACE was performed by the procedure described earlier. One modification was to increase the temperature in a reverse transcription reaction by using newly designed primers. First-strand cDNA was prepared from mRNA with MuscaFMRF-R2 at 55°C, about 10°C higher than that in the previous run. The PCR amplification reaction was performed with MuscaFMRF-R1 and AAP primers, and nested PCR was carried out with a newly designed *Musca fmrf* gene-specific primer MuscaFMRF-R0 (5′-AGCCCATGCGACCCACTGAGCTC TT-3′ corresponding to the nucleotide sequence 670–694 in Fig. 1) and AUAP. All other reactions were executed as mentioned earlier.

In situ Hybridization of fmrf mRNA Gene—Fixation of Musca Brains—Brains of 5-day-old houseflies *Musca domestica* were dissected under a binocular microscope and fixed in freshly made 4% formaldehyde, as paraformaldehyde, in 0.1 M phosphate buffer (pH 7.4) for 12 h at 4°C. Tissues were washed at 4°C with 0.01 M PBS containing 0.1% Tween 20 (denoted as PBST), dehydrated with a series of MeOH solutions (25, 50, 75% and then 2 × 100%) in PBST, and stored at −20°C until use.

Preparation of cRNA Probes for Musca fmrf and pdf mRNA Genes—To clarify the location of the cells expressing *fmrf* mRNA, a digoxigenin (DIG)-labelled *fmrf* cRNA probe was prepared. Using T7 RNA polymerase, an antisense *fmrf* cRNA probe labelled by digoxigenin (DIG)-UTP was produced *in vitro* from plasmid linearized with *Sal*I. The plasmid used involved the PCR product corresponding to *fmrf* cDNA of position 1159–1592 in the vector pBluescript II SK+. The reaction mixture of plasmid (1 μg), 5× buffer (4 μl; 0.2 M Tris–HCl (pH 8.0), 40 mM $MgCl_2$, 10 mM spermidine-$(HCl)_3$, 125 mM NaCl), 10× DIG RNA labelling mix (2 μl; 10 mM ATP, 10 mM CTP, 10 mM GTP, 6.5 mM UTP, 3.5 mM DIG-11-UTP (pH 7.5; Roche Diagnostics, Mannheim, Germany), 5 mM DTT (2 μl), an RNase inhibitor RNasin® (1 μl; Promega, Madison, WI, USA) and T7 RNA polymerase for antisense primer (2 μl, 100 U) was incubated at 37°C for 2 h. The reaction was terminated by adding 0.5 M EDTA (2 μl, pH 8.0). In order to precipitate DIG-labelled cRNA product, 4 M LiCl (2 μl) and ethanol (75 μl) was added and the solution was centrifuged at 17,000*g* for 20 min at 4°C. The residual pellet was washed with 70% ethanol and dried in the air. The pellet was eventually dissolved in 50% formamide (50 μl). The quality of the transcript was analysed by electrophoresis on a 1.5% agarose gel stained with ethidium bromide.

For double-labelled *in situ* hybridization, DIG-labelled *fmrf* cRNA prepared above was utilized as one of the probes. In addition, as a counterprobe, a fluorescein isothiocyanate (FITC)-labelled *pdf* cRNA probe was prepared. Using T7 RNA polymerase, antisense *pdf* cRNA probe labelled with FITC-UTP was prepared *in vitro* from the plasmid linearized with *Bam*HI, corresponding to the nucleotide positions 39–501 of *Musca pdf* (GenBank accession No. AB095922). *In vitro* transcription was performed using an FITC RNA labelling mix (Roche) instead of the DIG RNA labelling mix.

Whole-mount in situ Hybridization—Whole-mount *in situ* hybridization was performed essentially as described by Wilkinson (*30*) with several significant modifications. All the following procedures were performed at 25°C unless otherwise noted. Dehydrated tissues were rehydrated through a reverse series of MeOH–PBST solutions (75, 50, 25% MeOH, and 2× PBST). These re-hydrated tissues were permeabilized with 10 μg/ml proteinase K (Nacalai Tesque, Kyoto) at 37°C for 15 min, washed with aqueous glycine (2 mg/ml) for 5 min, and then washed twice with PBST. They were fixed in 0.2% glutaraldehyde/4% paraformaldehyde in PBST for 20 min, washed twice with PBST and incubated in PBST at 70°C for 50 min. After cooling on ice, tissues were treated with 6% H_2O_2 for 1 h, washed three times with PBS and incubated with pre-hybridization buffer (50% formamide, 5× SSC (pH 4.5), 1% SDS, 50 μg/ml yeast tRNA and 50 μg/ml heparin) at 70°C for 1 h. The pre-hybridization buffer was then replaced with hybridization buffer, *i.e.* a solution of pre-hybridization buffer containing a DIG-labelled cRNA probe, and the solution was incubated at 70°C for 16 h.

After hybridization, tissues were washed three times with solution I [50% formamide, 5× SSC (pH 4.5) and 1% SDS] at 70°C for 30 min, and once more with a 1:1 mixture of solutions I and II (solution II: solution I with no formamide) at 70°C for 10 min. The tissues were washed further three times with solution II for 5 min, and then incubated with solution II for 20 min. Washings were repeated twice with solution III [50% formamide, 2× SSC (pH 4.5) and 1% SDS] for 5 min at 70°C, three times more with solution III, but for 30 min each, and then with a TBST solution in which Tris-buffered saline (TBS; 150 mM NaCl, and 100 mM Tris–HCl, pH 7.5) contains 1% Tween 20. After blocking at 25°C for 1 h, in order to visualize mRNA-bound probe by immunocytochemical detection, tissues were treated with Fab fragments of sheep anti-DIG antibody directly conjugated to alkaline phosphatase (AP). This incubation was continued for 16 h at 4°C. Tissues were then washed successively four times with TBST for 5 min each and seven times for 1 h each. After washing twice with NTMT [100 mM NaCl, 100 mM Tris–HCl (pH 9.5), 50 mM $MgCl_2$ and 1% Tween 20] for 5 min, the antibody detection

reaction was performed by incubating the tissues in the substrate solution [NTMT with 0.33 mg/ml 4-nitro-blue tetrazolium chloride (NBT) and 0.17 mg/ml 5-bromo-4-chloro-3-indolylphosphate, BCIP] for 30 min in shaded light, and finally washed with TBST. Finally, whole tissues were mounted in glycerol–gelatin (Sigma, St Louis, MO, USA) and observed by light microscopy with an Olympus BX50.

Double-labelled in situ Hybridization—Double-labelled *in situ* hybridization was performed by means of the procedure used for whole-mount *in situ* hybridization with some modifications. Housefly brains were incubated in the hybridization solution containing both DIG-labelled *fmrf* cRNA probe and FITC-labelled *pdf* cRNA probe for 16 h at 70°C. After this hybridization reaction, tissues were washed as described for the whole-mount *in situ* hybridization and brains were subjected to the blocking reaction. After blocking at 25°C for 1 h, tissues were treated with anti-DIG-peroxidase (POD) Fab fragments (Roche) for 16 h at 4°C. Tissues were washed and DIG-labelled *fmrf* cRNA signals were amplified by TSA™ plus dinitrophenol (DNP) technology. Briefly, tissues were treated with DNP working solution for 10 min and washed. After blocking, tissues were incubated with anti-DNP-HRP Fab fragments and signals were visualized by the ImmunoPure® Metal Enhanced DAB (dimethylaminoazobenzene) Substrate kit (Pierce), which utilizes cobalt chloride and nickel chloride to produce a dark-brown precipitate in the presence of horseradish peroxidase (HRP). After washing with TBST, housefly brains were incubated with anti-FITC-AP Fab fragments for 16 h and then with the substrate solution (NTMT containing BCIP/NBT) for 30 min in shaded light. Eventually, the whole tissues were washed with TBST and mounted in glycerol–gelatin (Sigma) to observe by light microscopy as before.

Double-labelled in situ Hybridization of Drosophila fmrf and pdf mRNA Genes—Double-labelled *in situ* hybridization of *Drosophila* (Canton S) *fmrf* and *pdf* mRNA genes was carried out using a DIG-labelled *fmrf* cRNA probe and an FITC-labelled *pdf* cRNA probe, respectively. Antisense *pdf* cRNA probe labelled with FITC-UTP was prepared *in vitro* from the phagemid linearized with *Eco*RI. This ca. 600 bp probe corresponds to the whole *Drosophila pdf* mRNA (GenBank accession No. NM079793). Antisense *fmrf* cRNA probe labelled by DIG-UTP was prepared in a similar way from plasmid involving the PCR product corresponding to *Drosophila fmrf* cDNA (GenBank accession No. NM139501) of position 656–1473. Fixation followed by double-labelled *in situ* hybridization was performed under the same conditions for *Musca*.

RESULTS

Musca domestica fmrf cDNA—Degenerate primers for cDNA cloning were designed with reference to the sequence homology between FMRFamide peptides of *Drosophila* and *Calliphora vomitoria* (*28*, *31*, *32*). For the 3′ RACE method, three primers, PKQDFMRFG-F, QDFMRFGR-F and DNFMRFGR-F, were used to amplify the *Musca fmrf* gene. Several distinct gel bands were detected in each PCR reaction using these primers, and the nucleotide sequences of all the resulting products were analysed. In short, only when DNFMRFGR-F was used the fragment of *Musca fmrf* gene was obtained and this product was found to contain five copies of FMRF (corresponding to 274–325 in the final amino acid sequence). 3′ RACE and 5′ RACE experiments were performed on the basis of sequence information of this fragment.

A full-length cDNA clone was finally obtained, and the entire oligonucleotide structure was clarified. It comprises 1640 bp encoding a precursor protein of 388 amino acid residues (Fig. 1). Since the selected ATG codon and its adjacent nucleotide sequences fulfilled Kozak's consensus motif (*33*), the initiator codon ATG was assigned to position 214–216 as shown in Fig. 1. No additional ATG codon was found in the upstream 5′ UTR region. The program Signal P (http://www.cbs.dtu.dk/services/SignalP/) for predicting a signal peptide cleavage site showed that 21 amino acids from a selected Met should be a signal peptide.

Amino Acid Sequence Analysis of FMRFamide Peptides—The amino acid sequence converted from the oligonucleotide sequence of the *Musca fmrf* cDNA gene revealed that the gene encodes 17 FaRPs in total. At the most C-terminal side, the precursor contains a C-terminal free 14-mer peptide. At the N-terminal side, there is a 101-mer peptide (or protein) truncated by the 22-mer N-terminal signal peptide and the KR cleavage site. Consecutively, there follow an 11-mer peptide amide LRSLQENAMRW-NH_2(GKR) and then an 18-mer peptide amide SYESYOLNRNGL ADKSSV-NH_2(GR). All 17 FaRPs are present between this 18-mer peptide amide and C-terminal 14-mer peptide. They are encoded in tandem, being truncated by the amidation signal of GR at 16 sites and GK at one site (Fig. 2). As shown in Fig. 2, the size of the *Musca* FaRPs is relatively small, with amino acid residues 7–21.

Among total of 17 copies of FaRPs, there are four copies of NPGSQDFMRF-NH_2(GR) and two copies of SPGSQDFMRF-NH_2(GR) (Fig. 2). Interestingly, these peptides have exactly the same sequence of PGSQ DFMRF-NH_2(GR), and only the N-terminal amino acids N(=Asn) and S(=Ser) are different from each other. When we designate these peptides NPGSQDFMRF-NH_2(GR) and SPGSQDFMRF-NH_2(GR) as (*N*) and (*S*), respectively, they were found to be encoded successively in tandem as in the order of (*S*)–(*N*)–(*S*)–(*N*)–(*N*)–(*N*). Other 11 of the FaRPs have an N-terminal peptide sequence of MGFLSNHQVIRDSRGDN, SVGGSGGN DDN, ASGSSD, AGQDN, AAGQD, GSGQD, ASGGQD, APSGQD, PDN, TPAQSSD or TPTQSSD, as well as the C-terminal FMRF-NH_2(GR). In *D. melanogaster*, 8 different kinds of FaRPs, which total 13 copies, are encoded in a single gene (Fig. 2). Among them, only PDNFMRF-NH_2(GR) was found to be shared between the *Drosophila* and *Musca* FaRPs.

fmrf-Expressing Cells in Musca Brains—Whole-mount *in situ* hybridization was performed to identify the cells expressing *fmrf* mRNA. A DIG-labelled cRNA probe

Fig. 2. **Various FMRFamide-related peptides present in the precursor proteins of the housefly *Musca domestica* (A) and the fruit fly *Drosophila melanogaster* (B).** The signal peptides shown by dotted underline were predicted by program Signal P (http://www.cbs.dtu.dk/services/SignalP/). Dibasic amino acid cleavage sites KR are double-underlined. All 'FMRF' sequences are boxed. A solo 'GK' sequence present in *Musca* FMRF amide is underlined. Asterisks indicate a stop codon there.

was prepared to hybridize the *fmrf* mRNA gene at positions 1159–1592, which corresponds to the 3′ portion (1159–1380) of the protein-coding region and 3′ UTR (1381–1592). As shown in Fig. 3A, approximately four cell groups were identified for the *Musca* brain by this whole-mount *in situ* hybridization procedure. One large group, with two cell clusters each containing two large cells, was observed in the lateral neurons in each optic lobe (Fig. 3B), and two slightly bigger cells were observed on both sides of the tritocerebrum (Fig. 3C). A cell group of about 14 fairly small cells was observed in the dorsal area (Fig. 3D), while another group of 13 cells was in the subesophageal ganglion (Fig. 3E). The arrangement of these clusters is summarized in Fig. 4. In addition to the lateral neurons, most *fmrf* mRNAs are expressed in the central brain. No signals were detected when used sense *fmrf* mRNA probe as negative control (data not shown).

It is significant that some *Musca fmrf* mRNA-expressing cells appeared to locate in the same portion of the brain as in the *Musca* brain, containing *Musca pdf* mRNA-expressing cells. As previously reported (*13*), these are the lateral neurons of the optic lobe. There are two *pdf* expressing cell clusters in each optic lobe, one comprising four large cells and the other four small cells, as seen with double-labelled *in situ* hybridization, below. The results from *in situ* hybridization of *fmrf* mRNA show that the two *fmrf*-expressing cell clusters are located among the lateral neurons and that their cell sizes are similar to those of the large *pdf*-expressing cells.

Double-labelled in situ Hybridization of fmrf- and pdf-expressing Cells—In situ hybridization experiments carried out individually to detect *fmrf* and *pdf* mRNAs, raised the possibility that, among the *fmrf*-expressing cells, two pairs of lateral neurons could also express *pdf* mRNA (Fig. 4). To confirm whether or not *fmrf* and *pdf* mRNAs are co-expressed in the exact same cells, double-labelled *in situ* hybridization was performed using the DIG-labelled cRNA probe to detect *fmrf* mRNA and FITC-labelled cRNA probe for *pdf* mRNA (Fig. 5A). Both signals were found in the same region of fly's brain containing the lateral neurons, the anterior cortex of the medulla. However, as shown in Fig. 5B,

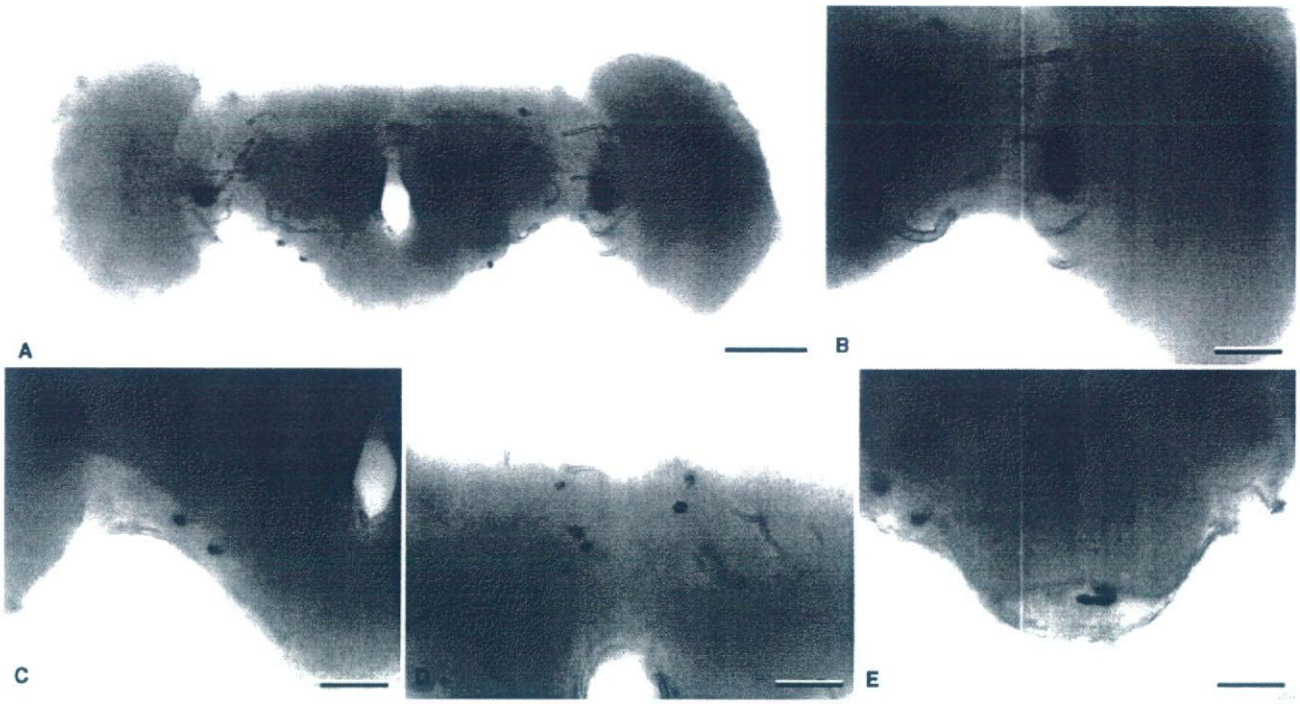

Fig. 3. **The whole-mount *in situ* hybridization for detection of *fmrf* mRNA in the brain of the housefly *Musca domestica*.** (A) A profile of whole brain with optic lobes (scale bar, 100 μm); and (B), (C), (D) and (E) expanded segmental views (scale bar, 50 μm). Observed cells are as follows: (B) two distinct cells in the lateral neurons in each optic lobe; (C) a single cell in the tritocerebrum; (D) approximately 14 cells in the dorsal area and (E) approximately 13 cells in the subesophageal ganglion.

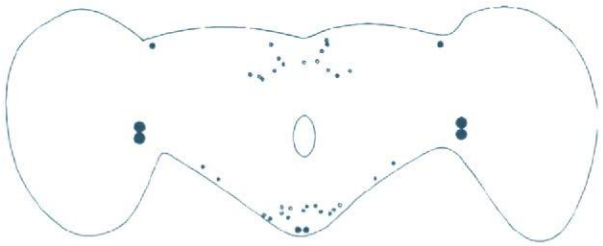

Fig. 4. **Schematic perspective drawing of the *fmrf* mRNA-expressing cells in the brain of the housefly *Musca domestica* detected by whole-mount *in situ* hybridization.** There are two pairs of four large cells among the lateral neurons, and two slightly bigger cells in the tritocerebrum. In addition, approximately 14 small cells are in the dorsal portion.

both brown and dark-blue signals never merged with each other. Two *fmrf*-expressing cells and all of *pdf*-expressing cells, four large and four small cells, were identified separately and individually in the lateral neurons. The *fmrf*-expressing cells revealed by brown signals were found more ventrally than the large *pdf*-expressing cells shown by dark-blue signals, and more lateral and dorsally than the small *pdf*-expressing cells. Given that the two signals nowhere merged, the *fmrf*-expressing cells are clearly different from the *pdf*-expressing cells.

The brains of *D. melanogaster* also exhibited non-merging signals of the *fmrf* mRNA hybridized by DIG-labelled cRNA probe and of the *pdf* mRNA hybridized by FITC-labelled cRNA probe. As shown in Fig. 6, with the FITC-labelled cRNA probe, *Drosophila pdf* mRNAs were observed in both large and small lateral neurons (*l*LNs and *s*LNs). When hybridized with DIG-labelled cRNA probe, *fmrf* mRNA-expressing cells were also found in the same region of the brain as the *pdf* mRNA-expressing *l*LNs and *s*LNs. However, again, the respective signals never merged, indicating that *fmrf*-expressing cells are clearly different from *pdf*-expressing cells.

DISCUSSION

Multiplicity of FMRFamide Peptides in the Amino Acid Sequence—Since the discovery of tetrapeptide FMRFamide, numerous members of the FaRP peptide family have been identified throughout the Metazoa. The *fmrf* mRNA was first clarified from an abdominal ganglion cDNA library of the marine mollusk *Aplysia californica* by a differential screening technique (*25*). Surprisingly, in addition to the FLRF tetrapeptide amide (=FLRFGR) and GYLRF pentapeptide amide (GYLRFGR), it encoded 28 FMRFs, the tetrapeptide amide FMRFGR, in tandem in a single gene. Multiple FaRPs are also encoded in other invertebrates, for instance, in the nematode *Caenorhabditis elegans*. *C. elegans* has no less than 20 FaRP precursor genes which encode a total of 56 FaRPs (*34*, *35*). No physiological significance of such diversity and multiplicity has yet been clarified.

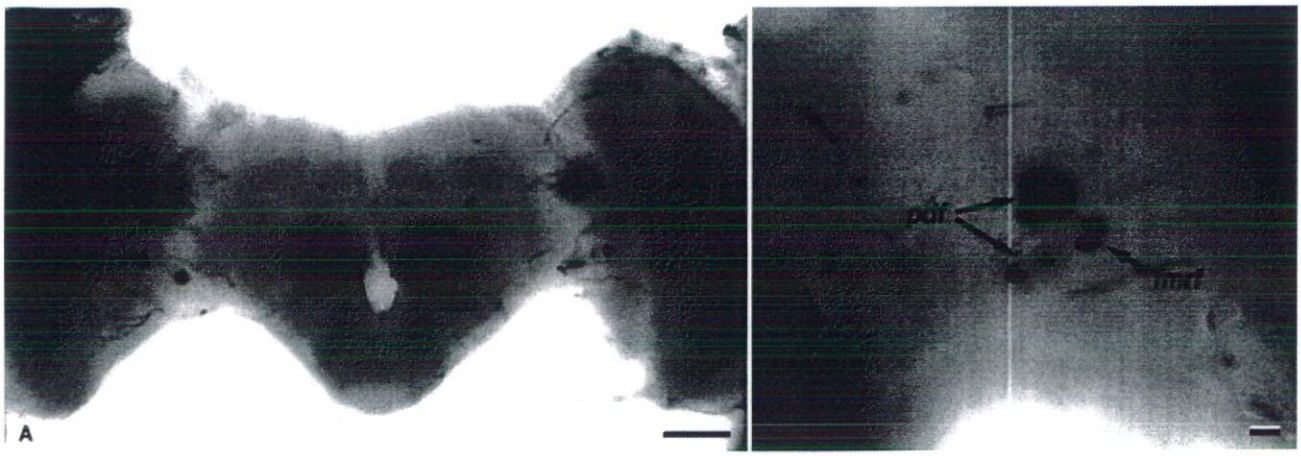

Fig. 5. **Double-labelled *in situ* hybridization of *fmrf* and *pdf* mRNAs in the brain of the housefly *Musca domestica*.** Brown signal indicates cells expressing *fmrf* mRNA, while dark-blue signal indicates those expressing the *pdf* mRNA. (A) Entire brain treated with double-labelled *in situ* hybridization (scale bar, 100 μm); and (B) expanded sectional view (scale bar, 20 μm).

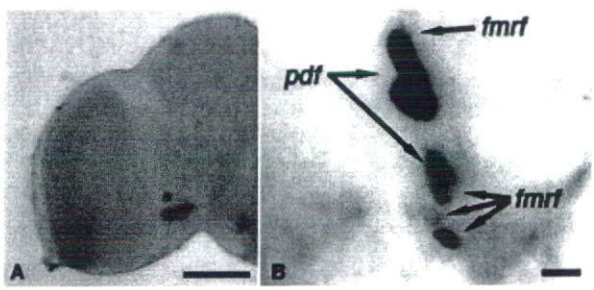

Fig. 6. **Double-labelled *in situ* hybridization of *fmrf* and *pdf* mRNAs in the brain of the fruit fly *Drosophila melanogaster*.** Brown signal indicates cells expressing *fmrf* mRNA, while dark-blue signal indicates those expressing the *pdf* mRNA. (A) Entire brain treated with double-labelled *in situ* hybridization (scale bar, 100 μm); and (B) expanded sectional view (scale bar, 20 μm).

In the EMBL/Genbank database, only two nucleotide sequences for FMRFamide peptides have been reported, the mRNAs of the fruit flies *D. melanogaster* and *D. virilis*. Indeed, such very limited information regarding the oligonucleotide sequences provided severe obstacles to the cDNA cloning of the housefly *fmrf* mRNAs, and required very sophisticated experimental strategies and primer design for the eventual successful cloning. For sufficient gene amplification, PCR should be carried out under the condition that there is an adequate number of target clones in the cDNAs that are reverse-transcribed. It was therefore a concern that the concentration of *fmrf* mRNA in the whole brain. In order to overcome this intrinsic problem, mRNAs were finally extracted from the thoracic ganglia. The fact that thirteen different FaRP peptides were actually isolated from the thoracic ganglia of the blowfly *Calliphora vomitoria* (*28*) prompted us to excise this tissue rather than the brain for the collection of concentrated *fmrf* mRNA. The difficulty in cDNA cloning further became clear when the amino acid sequence of the precursor protein of FMRFamide peptides was explored. Its sequence, particularly the sequences of FMRFamide peptides, was found to differ considerably from those of *D. melanogaster* (Fig. 7). The differences were remarkable; with only one FMRFamide peptide conserved between the two fly species, even though both are members of closely related clades of Diptera. It is evident that cDNA cloning of such a divergent gene is difficult.

When the amino acid sequences of precursor proteins translated from *Drosophila* and *Musca fmrf* mRNAs were compared (Fig. 2), these FaRP genes were found to show various disparities. First of all, the total numbers of copies of FMRFamide-containing peptides encoded in a single gene are different: 10 copies for *Drosophila* and 17 for *Musca*. Among the 17 *Musca* FMRFamide peptides, the peptides encoded at the most N-terminal side are 21- and 16-mer FMRFamides. All other FMRFamide peptides are rather short with 7–11 amino acid residues. Most FMRFamide peptides are truncated by GR at the both the N- and C-terminal sides, whereas the GR and GK sites truncate the most C-terminal TPTQSSDFMRFamide. Thus, there are 16 FMRFGR sequences in total and 1 FMRFGK in the same gene. Although the monobasic sites GR and GK are not always enzymatically cleavable (*36*), these are assumed to be the truncate sites for exclusive production of FMRFamide peptides. *Drosophila* has one longer-type (16-mer) and nine shorter-type (7–9-mer) FMRFamide peptides as shown in Fig. 7.

As to the FMRFamide peptides of the shorter type, there are remarkable differences in their primary structures. *Musca* FMRFamide encodes eight different 10-mer peptides, which contain a hexapeptide amide of QDFMRFamide in their C-terminus. The *Drosophila* FMRFamide precursor consists of six different peptides terminating with C-terminal QDFMRFamide, but in 9-mer peptides. These suggest an important role for the physiological functions of the QDFMRFamide moiety, presumably as an address code to specify and bind to specific receptors.

fmrf-Expressing Cells do not Express pdf—PDF peptide in *D. melanogaster* is present in several cell clusters

```
DmelanogasterFMRF MGIALMFLLALYQMQSAIHSEIIDTPN-YAGNSLQDADSQVSPS----QDNDLVDALLGN 55
DvililusFMRF      MGIALMFLLALYQMQSAIHSEIIETPSSYNDNSLLEAAAEEPNSRATASESDLLDGLMST 60
MuscaFMRF         MVAPLLVFLFSLQLCHTTSWAYVGGNS-LNSNSLHASYSEFPAGTSNEVPEDAANGQDDN 59
                  *  .*:.:*   *:  :     :   .   .***  : :: . .      .*  :.  ..

DmelanogasterFMRF DQ----------------TERAELEFRHPISVIGIDYSKNAVVLHFQKHGRKPRYKYDP 98
DvililusFMRF      DNP--------------NPEQQTELEFRYPISAIGIGYAKNSVVLRFQKHARKQNFKYDP 106
MuscaFMRF         DDSQLTEPNDNNAPLVQSIDDETEMQFPKPIQWVSIDHLRNSIILRFQNPTPKILNKLDP 119
                  *:                  :.:*::*  **. :.*.: :*:::*:**:   *   * **

DmelanogasterFMRF ELEAKRRSVQDNFMHFGKRQAEQLPPEGSYAGSDELEGMAKRAAMDRYGRDPKQD-FMRF 157
DvililusFMRF      DYEMKRKSLQDNFMHFGKRQAEQLP-QATGPG---YYECIKRSAMDRYGRDPKQD-FMRF 161
MuscaFMRF         EEMKRLRSLQENAMRWGKRSYESYPLNRNGLADKSSVGRMGFLSNHQVIRDSRGDNFMRF 179
                  :   : :*:*:* *::***. *. * : .  .          : .:  **.: * ****

DmelanogasterFMRF GRDP------KQDFMRFGRDPKQDFMRFGRDPKQDFMRFGRDPKQDFMRFGRTPAADFMR 211
DvililusFMRF      GRAP------PSDFMRFGRAP-----------------------------------SDFMR 181
MuscaFMRF         GRSVGGSGGNDDNFMRFGRASGSS----------DFMRFGRAGQDNFMRFGRAAGQDFMR 229
                  **          .:****** .                                  ****

DmelanogasterFMRF FGRTPAEDFMRFGRS---DNFMRFGRSP--HEDVR---SP-KQDFMRFGR---PDNFMRF 259
DvililusFMRF      FGRDPSQDFMRFGRS---DNFMRFGRNLNFHEELR---SP-KQDFMRFGR---PDNFMRF 231
MuscaFMRF         FGRGSGQDFMRFGRSPGSQDFMRFGRNPGSQDFMRFGRSPGSQDFMRFGRNPGSQDFMRF 289
                  *** ..:********   ::******.   :: :*   ** .********   .::****

DmelanogasterFMRF GRS-RPQDFVRSGK--MDSNFIRFGKS------LKPAAPESKPVKSNQGN--PGER---S 305
DvililusFMRF      GRS-APTEFERNGK--MDSNFMRFGKRSGVMAKLTKSQLQQNKLTTADGKQQPAEEG--N 286
MuscaFMRF         GRNPGSQDFMRFGRNPGSQDFMRFGRASGGQDFMRFGRAPSGQDFMRFGRPDNFMRFGRT 349
                  **.  . :* * *:   ..:*:***:       :  .   .       *.     .   .

DmelanogasterFMRF PVDKAMTELFKKQELQDQ-------------QVKNGAQATTTQDGSVEQDQFFGQ 347
DvililusFMRF      PTDKAISMLFNKHQQQQQQQQGQRLQQEDRQQMKSSAEQNNLEEASVEQ--FYEP 339
MuscaFMRF         PAQSSDFMRFGRTPTQSS----------DFMRFGKSLDKSENKTSDLQK------ 388
                  *.:.:    * :   *..             :. .. : .  : ..:::
```

Fig. 7. **The sequence alignment of fly FMRFamide precursor proteins.** '*': Residues in that column are identical in all sequences in the alignment. ':': Conserved substitutions are observed. '.': Semi-conserved substitutions are observed.

of clock cells that express the clock gene *period*. There is clear evidence that the *pdf*-mutated flies show abnormal circadian rhythm behaviour (*11*), although these mutant flies do not show arrhythmic, completely random activity. Residual rhythmicity in *pdf* mutants and the residual *period*-expressing cells which lack *pdf* peptide likely reflects the activity of other neurotransmitters. It has also been reported that certain mosaic flies for the neuropeptide amidating enzyme were less rhythmic than *pdf* mutants (*37*). This suggests that multiple amidated neuropeptides other than PDF function in daily locomotor rhythms.

Together with these suggestions, several other investigations strongly suggested that (*1*) FMRFamide peptides are a neuropeptide involved in circadian rhythm (*20*); and (*2*) FMRFamide peptides are co-expressed or co-localized with PDF peptide in the same neurons (*20–23*). However, the latter possibility was clearly excluded in the present study by means of double-labelled *in situ* hybridization, at least for the two flies *M. domestica* and *D. melanogaster*. In *Musca* brains, a cell cluster of two *pdf*-expressing cells and two *fmrf*-expressing cells is present symmetrically in the lateral regions of each optic lobe. These *fmrf*-expressing cells and *pdf*-expressing cells lie in close proximity to each other, but apparently do not overlap or merge, and thus are different neurons. The same was also clear in the *Drosophila* brains.

Although double-immunolabelling in insect brains using anti-crustacean β-PDH and anti-FMRFamide antibody suggested that insect PDF and FMRFamide-like peptides might co-exist in the same cells (*20–23*), the present study demonstrated non-overlapping expression of *pdf* and *fmrf* mRNA genes. We analysed previously the specificity of anti-crustacean β-PDH antibody (*19*), and evidenced that the PDF-expressing neurons are the same cells detected by *in situ* hybridization (*16*, *17*). The present results suggest possible cross-reactivity to unknown peptides of anti-FMRFamide antibody.

The mechanism of cell-specific transcriptional regulation of the *Drosophila fmrf* gene has been clearly

characterized (*38*). Transcriptional control elements required for spatial and temporal regulation of *fmrf* gene expression seem to be distributed over 8 kb of genomic DNA and several enhancer regions have been identified in the 5′ region of the *fmrf* gene. These cell-specific expression patterns presumably indicate the importance of the gene product, the multiple FaRPs in the insect nervous system, some of which perhaps function in circadian rhythms. If FMRFamide peptides were involved in the molecular mechanisms underlying circadian rhythms, they and their gene would be predicted to exhibit certain circadian prerequisites: for instance (*1*) peptides in secretary vesicles may exhibit a circadian rhythmicity; (*2*) mRNA may co-express in a neuron with *period* mRNA or (*3*) mRNA production may exhibit circadian rhythmicity. Experiments to reveal these points are in progress in our laboratory.

We thank Prof. Ian A. Meinertzhagen, Dalhousie University, Canada, for reading the manuscript. This study was supported by grants-in-aid from the Ministry of Education, Science, Sports and Culture in Japan; grant 11878113 to Y.S., and grant 1287115 & 18570075 to M.S., and in part by Health and Labour Sciences Research Grants for Research on Risk of Chemical Substances from the Ministry of Health, Labor and Welfare of Japan to Y.S.

REFERENCES

1. Price, D.A. and Greenberg, M.J. (1977) Structure of a molluscan cardioexcitatory neuropeptide. *Science* **197**, 670–671
2. Nichols, R., Schneuwly, S.A., and Dixon, J.E. (1988) Identification and characterization of *Drosophila* homologue to the vertebrate neuropeptide cholecystokinin. *J. Biol. Chem.* **263**, 12167–12170
3. Holman, G.M., Cool, B.J., and Nachman, R.J. (1986) Isolation, primary structure and synthesis of leucomyosuppressin, an insect neuropeptide that inhibits spontaneous contractions of the cockroach hindgut. *Comp. Biochem. Physiol.* **85C**, 329–333
4. Nichols, R. (1992) Isolation and structural characterization of *Drosophila* TDVDHVFLRFamide and FMRFamide-containing neural peptides. *J. Mol. Neurosci.* **3**, 213–218
5. Rao, K.R., Mohrherr, C.J., Riehm, J.P., and Zahnow, C.A. (1987) Primary structure of an analog of crustacean pigment-dispersing hormone from the lubber grasshopper *Romalea microptera*. *J. Biol. Chem.* **262**, 2672–2675
6. Stengl, M. and Homberg, U. (1994) Pigment-dispersing hormone-immunoreactive neurons in the cockroach *Leucophaea maderae* share properties with circadian pacemaker neurons. *J. Comp. Physiol.* [A] **175**, 203–213
7. Pyza, E. and Meinertzhagen, I.A. (1996) Neurotransmitters regulate rhythmic size changes amongst cells in the fly's optic lobe. *J. Comp. Physiol.* [A] **178**, 33–45
8. Meinertzhagen, I.A. and Pyza, E. (1996) Daily rhythms in cells of the fly's optic lobe: taking time out from the circadian clock. *Trends Neurosci.* **19**, 285–291
9. Mertens, I., Vandingenen, A., Johnson, E.C., Shafer, O.T., Li, W., Trigg, J.S., De Loof, A., Schoofs, L., and Taghert, P.H. (2005) PDF receptor signaling in *Drosophila* contributes to both circadian and geotaxic behaviors. *Neuron* **48**, 213–219
10. Petri, B. and Stengl, M. (1997) Pigment-dispersing hormone shifts the phase of the circadian pacemaker of the cockroach *Leucophaea maderae*. *J. Neurosci.* **17**, 4087–4093
11. Renn, S.C.P., Park, J.H., Rosbash, M., Hall, J.C., and Taghert, P.H. (1999) A *pdf* neuropeptide gene mutation and ablation of PDF neurons each cause severe abnormalities of behavioral circadian rhythms in *Drosophila*. *Cell* **99**, 791–802
12. Park, J.H., Helfrich-Föster, C., Lee, G., Liu, L., Rosbash, M., and Hall, J.C. (2000) Differential regulation of circadian pacemaker output by separate clock genes in *Drosophila*. *Proc. Natl. Acad. Sci. USA* **97**, 3608–3613
13. Helfrich-Förster, C., Täuber, M., Park, J.H., Muhlig-Versen, M., Schneuwly, S., and Hofbauer, A. (2000) Ectopic expression of the neuropeptide pigment-dispersing factor alters behavioral rhythms in *Drosophila melanogaster*. *J. Neurosci.* **20**, 3339–3353
14. Shirasu, N., Shimohigashi, Y., Tominaga, Y., and Shimohigashi, M. (2003) Molecular cogs of the insect circadian clock. *Zool. Sci.* **20**, 947–955
15. Chuman, Y., Matsushima, A., Sato, S., Tomioka, K., Tominaga, Y., Meinertzhagen, I.A., Shimohigashi, Y., and Shimohigashi, M. (2002) cDNA cloning and nuclear localization of the circadian neuropeptide designated as pigment-dispersing factor PDF in the cricket *Gryllus bimaculatus*. *J. Biochem.* **131**, 895–903
16. Matsushima, A., Yokotani, S., Lui, X., Sumida, K., Honda, T., Sato, S., Kaneki, A., Takeda, Y., Chuman, Y., Ozaki, M., Asai, D., Nose, T., Onoue, H., Ito, Y., Tominaga, Y., Shimohigashi, Y., and Shimohigashi, M. (2003) Molecular cloning and circadian expression profile of insect neuropeptide PDF in black blowfly, *Phormia regina*. *Lett. Pept. Sci.* **10**, 419–430
17. Matsushima, A., Sato, S., Chuman, Y., Takeda, Y., Yokotani, S., Nose, T., Tominaga, Y., Shimohigashi, M., and Shimohigashi, Y. (2004) cDNA cloning of the housefly pigment-dispersing factor (PDF) precursors protein and its peptide comparison among the insect circadian neuropeptides. *J. Pept. Sci.* **10**, 82–91
18. Sato, S., Chuman, Y., Matsushima, A., Tominaga, Y., Shimohigashi, Y., and Shimohigashi, M. (2002) A circadian neuropeptide, pigment-dispersing factor – PDF, in the last summer cicada *Meimuna opalifera*: cDNA cloning and immunocytochemistry. *Zool. Sci.* **19**, 821–828
19. Honda, T., Matsushima, A., Sumida, K., Chuman, Y., Sakaguchi, K., Onoue, H., Meinertzhagen, I.A., Shimohigashi, Y., and Shimohigashi, M. (2006) Structural isoforms of the circadian neuropeptide PDF expressed in the optic lobes of the cricket *Gryllus bimaculatus*: Immunocytochemical evidence from specific monoclonal antibodies. *J. Comp. Neurol.* **499**, 404–421
20. Pyza, E. and Meinertzhagen, I.A. (2003) The regulation of circadian rhythms in the fly's visual system: involvement of FMRFamide-like neuropeptides and their relationship to pigment dispersing factor in *Musca domestica* and *Drosophila melanogaster*. *Neuropeptides* **37**, 277–289
21. Homberg, U., Davis, N.T., and Hildebrand, J.G. (1991) Peptide-immunocytochemistry of neurosecretory cells in the brain and retrocerebral complex of the sphinx moth *Manduca sexta*. *J. Comp. Neurol.* **303**, 35–52
22. Nässel, D.R., Shiga, S., Mohrherr, C.J., and Rao, K.R. (1993) Pigment-dispersing hormone-like peptide in the nervous system of the flies *Phormia* and *Drosophila*: Immunocytochemistry and partial characterization. *J. Comp. Neurol.* **331**, 183–198
23. Settembrini, B.P. and Villar, M.J. (2005) FMRFamide-like immunocytochemistry in the brain and aubesophageal ganglion of *Triatoma infestans* (Insecta: Heteroptera). Coexpression with β-pigment-dispersing hormone and small cardioactive peptide. *Cell Tissue Res.* **321**, 299–310
24. Schaefer, M., Picciotto, R., Thane, K., Kaldany, R.R., Taussing, R., and Scheller, R.H. (1985) *Aplysia* neurons express a gene encoding multiple FMRFamide neuropeptides. *Cell* **41**, 457–467

25. Schneider, L.E. and Taghert, P.H. (1988) Isolation and characterization of a *Drosophila* gene that encodes multiple neuropeptides related to Phe-Met-Arg-Phe-NH_2 (FMRFamide). *Proc. Natl. Acad. Sci. USA* **85**, 1993–1997
26. Taghert, P.H. and Schneider, L.E. (1990) Interspecific comparison of a *Drosophila* gene encoding FMRFamide-related neuropeptides. *J. Neurosci.* **10**, 1929–1942
27. Frohman, M.A., Dush, M.K., and Martin, G.R. (1988) Rapid production of full-length cDNAs from rare transcripts: amplification using a single gene-specific oligonucleotide primer. *Proc. Natl. Acad. Sci. USA* **85**, 8998–9002
28. Duve, H., Johnsen, A.H., Sewell, J.C., Scott, A.G, Orchard, I., Rehfeild, J.F., and Thorpe, A. (1992) Isolation, structure, and activity of -Phe-Met-Arg-Phe-NH_2 neuropeptides (designated calliFMRFamides) from the blowfly *Calliphora vomitoria*. *Proc. Natl. Acad. Sci. USA* **89**, 2326–2330
29. Don, R.H., Cox, P.T., Wainwright, B.J., Baker, K., and Mattick, J.S (1991) 'Touchdown' PCR to circumvent spurious priming during gene amplification. *Nucleic Acids Res.* **19**, 4008
30. Wilkinson, D.G. (Ed.) (1999) *In Situ Hybridization: A Practical Approach*, 2nd edn, Oxford University Press, Oxford
31. Orchard, I., Lange, A.B., and Bendena, W.G. (2001) FMRFamide-related peptides: a multifunctional family of structurally related neuropeptides in insects. *Adv. Insect Physiol.* **28**, 267–329
32. Nässel, D.R. (2002) Neuropeptides in the nervous system of *Drosophila* and other insects: multiple roles as neuromodulators and neurohormones. *Prog. Neurobiol.* **68**, 1–84
33. Kozak, M. (1999) Initiation of translation in prokaryotes and eukaryotes. *Gene* **234**, 187–208
34. Li, C., Kim, K., and Nelson, L.S. (1999) FMRFamide-related neuropeptide gene family in *Caenorhabditis elegans*. *Brain Res.* **848**, 26–34
35. Li, C., Nelson, L.S., Kim, K., Nathoo, A., and Hart, A.C. (1999) Neuropeptide gene families in the nematode *Caenorhabditis elegans*. *Ann. N.Y. Acad. Sci.* **897**, 239–252
36. Veenstra, J.A. (2000) Mono- and dibasic proteolytic cleavage sites in insect neuroendocrine peptide precursors. *Arc. Insect Biochem. Physiol.* **43**, 49–63
37. Taghert, P.H., Hewes, R.S., Park, J.H., O'Brien, M.A., Han, M., and Peck, M.E. (2001) Multiple amidated neuropeptides are required for normal circadian locomotor rhythms in *Drosophila*. *J. Neurosci.* **21**, 6673–6686
38. Benveniste, R.J. and Taghert, P.H. (1999) Cell type-specific regulatory sequences control expression of the *Drosophila* FMRF-NH_2 neuropeptide gene. *J. Neurobiol.* **38**, 507–520

J. Biochem. **142,** 517–524 (2007)
doi:10.1093/jb/mvm158

Structural Evidence for Endocrine Disruptor Bisphenol A Binding to Human Nuclear Receptor ERRγ

Ayami Matsushima[1], Yoshimitsu Kakuta[2], Takamasa Teramoto[2], Takumi Koshiba[3], Xiaohui Liu[1], Hiroyuki Okada[1], Takatoshi Tokunaga[1], Shun-ichiro Kawabata[3], Makoto Kimura[2] and Yasuyuki Shimohigashi[1,*]

[1]Laboratory of Structure-Function Biochemistry, Department of Chemistry, Research-Education Centre of Risk Science, Faculty and Graduate School of Sciences; [2]Laboratory of Biochemistry, Department of Agricultural Chemistry, Faculty and Graduate School of Agriculture; and [3]Laboratory of Life Biochemistry, Department of Biological Science, Faculty of Sciences, Kyushu University, Fukuoka 812-8581, Japan

Received May 30, 2007; accepted July 25, 2007; published online August 30, 2007

Many lines of evidence reveal that bisphenol A (BPA) functions at very low doses as an endocrine disruptor. The human estrogen-related receptor γ (ERRγ) behaves as a constitutive activator of transcription, although the endogenous ligand is unknown. We have recently demonstrated that BPA binds strongly to ERRγ (K_D = 5.5 nM), but not to the estrogen receptor (ER). BPA preserves the ERRγ's basal constitutive activity, and protects the selective ER modulator 4-hydroxytamoxifen from its deactivation of ERRγ. In order to shed light on a molecular mechanism, we carried out the X-ray analysis of crystal structure of the ERRγ ligand-binding domain (LBD) complexed with BPA. BPA binds to the receptor cavity without changing any internal structures of the pocket of the ERRγ-LBD apo form. The hydrogen bonds of two phenol-hydroxyl groups, one with both Glu275 and Arg316, the other with Asn346, anchor BPA in the pocket, and surrounding hydrophobic bonds, especially with Tyr326, complete BPA's strong binding. Maintaining the 'activation helix' (helix 12) in an active conformation would as a result preserve receptor constitutive activity. Our results present the first evidence that the nuclear receptor forms complexes with the endocrine disruptor, providing detailed molecular insight into the interaction features.

Key words: binding assay, bisphenol A, estrogen-related receptor γ (ERRγ), nuclear receptor, X-ray crystal structure.

Abbreviations: BPA, bisphenol A; CBB, Coomassie brilliant blue; CHAPS, 3-[3-(cholamidopropyl)dimethylammonio]-1-propanesulfonic acid; DES, diethylstilbestrol; ER, estrogen receptor; ERR, estrogen-related receptor; ERE, estrogen response element; ERRE, ERR-response element; LBD, ligand-binding domain; MALDI-TOF, matrix-assisted laser desorption ionization time-of-flight; NR, nuclear receptor; 4-OHT, 4-hydroxytamoxifen; and PCR, polymerase chain reaction.

Bisphenol A (BPA), 2,2-bis(4-hydroxyphenyl)propane, has a symmetrical chemical structure of HO-C_6H_4-$C(CH_3)_2$-C_6H_4-OH. BPA is used mainly in the production of polycarbonate plastics and epoxy resins. Its worldwide manufacture is ~3.2 million metric tons per year. BPA had been acknowledged as an estrogenic chemical able to interact with human estrogen receptors (ERs) (*1*, *2*). In recent years, many lines of evidence reveal that BPA functions at its very low doses as an endocrine disruptor (*3–7*).

All of these so-called 'low-dose effects' of BPA have been explained as the output effects of steroid hormone receptor ERs (*8*). However, since BPA's binding to ER and hormonal activity is extremely weak, 1,000–10,000 times lower than for natural hormones, the intrinsic significance of low-dose effects has been intangible and obscure. BPA's low-dose effects have been peer-reviewed by the National Toxicology Program of the United States (*9*), and extensively reviewed by vom Saal and Hughes (*7*). The discrepancy on low-dose effects prompted us to enquire whether BPA may interact with nuclear receptors (NRs) other than ER, and as a BPA receptor we have recently identified the human estrogen-related receptor γ (ERRγ) (*10*).

The ERRγ belongs to the orphan subfamily of NRs (*11*), all members of which (ERRα, ERRβ and ERRγ) are closely related to ERs (*12*, *13*). ERRγ behaves as a constitutive activator of transcription, presumably with intrinsic roles in differentiation and maturation of the foetal brain. Although the endogenous ligand is unknown, we have shown that BPA binds strongly to ERRγ, but not to ER (*10*). BPA preserves the ERRγ's basal constitutive activity, and protects the selective ER modulator 4-hydroxytamoxifen (4-OHT) from its deactivation of ERRγ.

In order to explain such BPA's activities at the structural basis, we carried out the crystallization of the ERRγ ligand-binding domain (LBD) complexed with BPA. We here report the structure of the complex and shed light on a molecular mechanism between BPA and

*To whom correspondence should be addressed. Tel: +81-92-642-2584; Fax: +81-92-642-2584;
E-mail: shimoscc@mbox.nc.kyushu-u.ac.jp

ERRγ-LBD. This is the first straight evidence that the nuclear receptor forms a complex with the endocrine disruptor BPA. In the interaction with the receptor ERRγ, BPA was demonstrated to act as an inverse antagonist against 4-OHT's inverse agonist activity.

MATERIALS AND METHODS

Materials—3-[3-(Cholamidopropyl)dimethylammonio]-1-propanesulfonic acid (CHAPS), EDTA, HEPES and γ-globulin were obtained from Sigma (St Louis, MO, USA). Glycerol was from Nacalai Tesque (Kyoto), and all other chemicals used were of analytical grade and purchased from Wako (Osaka).

Methods—The concentration of nuclear receptor protein was estimated by the Bradford method (*14*) using the protein assay solution with Coomassie brilliant blue (CBB) (Nacalai Tesque). Mass spectra of proteins were measured on a mass spectrometer Voyager™ DE-PRO (PerSeptive Biosystems Inc., Framingham, MA, USA) using the matrix-assisted laser desorption ionization time-of-flight (MALDI-TOF) method.

Construction of Recombinant Plasmid—The cDNA fragment encoding human ERRγ-LBD (corresponding to amino acid residues 222–458) were generated by polymerase chain reaction (PCR) from kidney QUICK-Clone™ cDNA (Clonetech, Mountain View, CA, USA) using specific primers. The amplified product was cloned into the expression vector pGEX 6P-1 (Amersham Biosciences, Piscataway, NJ, USA) using *Eco*RI and *Xho*I restriction enzyme sites to express the product as a glutathione *S*-transferase (GST) fusion protein.

Site-directed Mutagenesis of ERRγ—The constructed plasmid were served as a template for Ala-substituted mutants. The PCR method was carried out to introduce the single-point mutations by using a series of overlapping sense and antisense primer pairs. The PCR fragments containing the E275A, M306A, L309A, R316A, Y326A, N346A and F435A mutations were cut with *Eco*RI and *Xho*I, and then subcloned into the expressing vector pGEX 6P-1.

Saturation Binding Assay—Saturation binding assay was conducted essentially as reported (*15*) at 4°C overnight to minimize degradation of the ligand receptor complex in a final volume of 100 μl of binding buffer [10 mM HEPES (pH 7.5), 50 mM NaCl, 2 mM $MgCl_2$, 1 mM EDTA, 2 mM CHAPS and 2 mg/ml γ-globulin]. GST-ERRγ-LBD of 30–3000 ng and [^{3}H]BPA (185 GBq/mmol, America Radiolabeled Chemicals Inc., St Louis, MO, USA) with or without addition of unlabelled BPA (final concentration of 10 μM) to quantify the non-specific binding. Free radio-ligand was removed by centrifugation (4°C, 10 min, 14,000 r.p.m.) or filtration after incubation with 100 μl of 1% dextran-coated charcoal (Sigma, St Louis, MO, USA) in PBS (pH 7.4) for 10 min at 4°C. Specific binding of [^{3}H]BPA was calculated by subtracting the non-specific binding from the total binding.

Protein Expression and Purification—GST fusion protein of the ERRγ-LBD was expressed by using *Escherichia coli* BL21 as described previously (*10*). Purification was carried out by using an affinity column of glutathione-sepharose 4B (Amersham Biosciences). GST was cleaved on the resin by using a specific enzyme, PreScission Protease (Amersham Biosciences), for 4 h at 4°C. After incubation, ERRγ-LBD was eluted and its concentration determined by the Bradford method using a CBB solution (*14*).

Crystallization of Protein Complex Followed by X-Ray Data Collection and Processing—Purified ERRγ-LBD was concentrated by ultrafiltration. Co-crystallization with a 3-fold molar excess of BPA was carried out with the hanging drop vapour diffusion method. The crystals used for data collection were from a drop of 2 μl of ERRγ-LBD solution mixed with BPA and 2 μl of reservoir solution (50 mM HEPES pH 7.5, 0.75 M sodium citrate and 5% glycerol). For data collection, crystals were transferred into a cryoprotectant solution containing 24% glycerol in reservoir solution, then mounted in a nylon loop and flash-frozen in a nitrogen stream at 100 K. X-ray diffraction data were collected at the beamline BL38B1, SPring-8 (Hyogo, Japan). The data were integrated and scaled using the HKL*2000* package (*16*).

Structure Determination and Refinement—A monomer model of ERRγ-LBD/4-OHT (1S9Q) was used as a search molecule for molecular replacement using MOLREP (*17*) in CCP4 (*18*). The position of the monomer in the asymmetric unit was located and the structure refined at 1.6 Å using REFMAC5 (*19*) in CCP4. Manual adjustment and rebuilding of the model including BPA and water molecules were performed using the program Coot (*20*). The final model contained residues 232–458 of ERRγ, one BPA, three glycerol and 387 water molecules. Multiple conformers were applied to Lys236, Ser239, Ile249, Tyr250, Val278, Lys284, Ser290, Met298, Ser303, Ser319, Ser358, Ile382, Gln389, Asp393, Gln400, Asp401, Gln406, His407, Met419, Ser428, Gln433 and Leu454. The final model was validated with PROCHECK (*21*). Date collection and structure refinement statistics are summarized in Table 1.

Minimum-energy Calculations—For the energy calculations of the geometry optimization of BPA, the conventional Hartree–Fock (HF) method was used on a computer program Gaussian (v. 03) with the 6-31G(d, p) basis set.

RESULTS AND DISCUSSION

Dimeric Structure of ERRγ-LBD—The crystals usable for data collection were obtained from a ERRγ-LBD solution mixed with BPA in the following reservoir solution: 50 mM HEPES pH 7.5, 0.75 M sodium citrate and 5% glycerol. We solved the crystal structure of the resulting ERRγ-LBD in a complex with BPA at a resolution of 1.6 Å (space group $P4_12_12$) (Table 1). The ERRγ-LBD crystallized in homodimeric form using crystallographic 2-fold symmetry, indicating that BPA binding does not interfere with homodimer formation (Fig. 1A). Homodimer formation of the purified ERRγ-LBD is also observed by MALDI-TOF mass spectrometry (Fig. 2), in agreement with the reported homodimeric binding of ERRs to DNA (*22*). A BPA molecule in the complex with ERRγ-LBD is defined very well from its electron density (Fig. 1B).

Table 1. **Data collection and refinement statistics for X-ray crystal analysis of the ERRγ. LBD complexed with BPA.**

Data set	
Space group	$P4_12_12$
Unit cell parameters	$a = 64.05$ Å
	$b = 64.05$ Å
	$c = 136.87$
Data collection	
Beam line	SPring-8 BL38B1
Wavelength (Å)	1.0
Resolution range (Å)	28.06–1.60
Number of reflections	
Observed	433–326
Unique	36;414
R_{sym} [a,b]	0.058 (0.349)
I/σ (I)[a]	40.4 (8.2)
Completeness (%)	99.6
Refinement statistics	
Resolution range (Å)	28.06–1.60
Number of reflections	36,414
Working set	34,493
Test set	1,921
Completeness (%)	99.6
R_{cryst} [c] (%)	16.9
R_{free} [d] (%)	19.7
Root mean square deviations	
Bond length (Å)	0.012
Bond angles (°)	1.333
Average B-factor (Å^2)	
Protein	18.9
BPA	15.5
Glycerol	39.1
Water	35.3
Number of atoms	2,357
Protein	1,935
BPA	17
Glycerol	18
Water	387
Ramachandran analysis	
Most favoured (%)	94.8
Allowed (%)	5.2
Generously allowed (%)	0.0
Disallowed (%)	0.0

[a]Values in parentheses are for the highest resolution shell. [b]$R_{sym} = \sum(-\langle I\rangle)/\sum\langle I\rangle$, where I is the intensity measurement for a given reflaction and $\langle I\rangle$ is the average intensity for multiple measurements of this reflaction. [c]$R_{cryst} = \sum|F_{obs} - F_{cal}|\sum F_{obs}$, where F_{obs} and F_{cal} are observed and calculated structure factor amplitudes. [d]R_{free} value was calculated for R_{cryst}, using only an undefined subset of reflection data (5%).

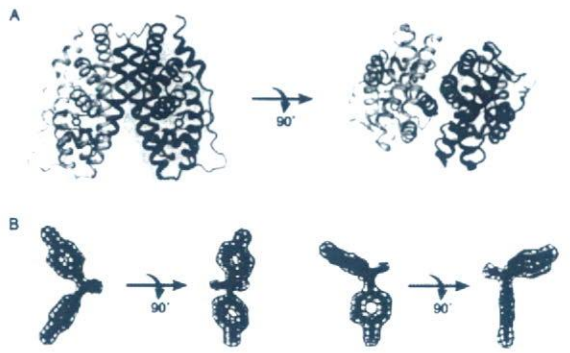

Fig. 1. **BPA/ERRγ-LBD complex.** (A) The panoramic view of whole-sphere BPA/ERRγ-LBD homodimer complex. Each panel shows the 3D-structure pictured from the top with 90° rotation. One molecule of BPA is in each ERRγ-LBD. BPA is shown in red colour. Characteristic α-helices are shown in distinctive colours; *i.e.* H10 in a dimerization interface, blue; H12 in an activation conformation, purple. (B) BPA bound to the ERRγ-LBD fitted into omitted Fo–Fc electron density maps at a level of 4.0 sigma. Right-side two panels show the aromatic face of BPA-A ring in a 90° rotation. Left-side two panels show the whole figure of the BPA molecule in a 90° rotation.

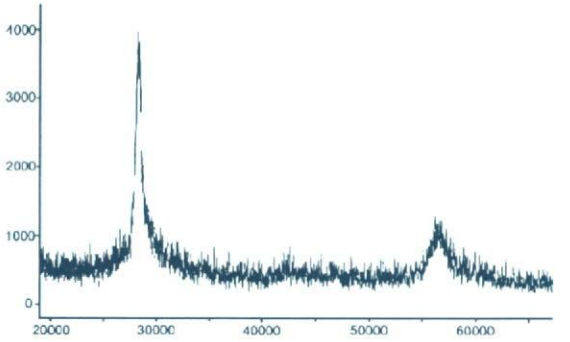

Fig. 2. **Dimer formation detected by MALDI-TOF mass spectrometry.** The peak of monomer emerges around 27,600 (calculated mass number [MH$^+$] of ERRγ-LBD: 27578.67), while the dimer peak is found at around 55,200.

ERRγ binds to the ERR-response element (ERRE), but as a monomer. ERRγ can also bind to functional estrogen response elements (EREs) in ER target genes, suggesting a possible overlap between ERR and ER action (*12*). Homodimers formed by the hydrophobic interactions between the interfaces of α-helix 10 (H10), which is supported by α-helix 7 (H7). Thus, in a homodimer, four α-helices are arranged in tandem to form the sequence H7–H10–H10–H7 (Fig. 1A, right). In the dimerization interface of H10–H10, such amino acid pairs as Pro422–*Pro422*, Arg425–*Gln426* and Gln426–*Arg425* appear to make a specific intermolecular interaction (Fig. 3A; the residues in italic characters are of the second molecule of ERRγ dimer). At the interface between H7 and H10, Tyr356–Thr420 and Met359–Met417 pairs are likely to underlie the intramolecular interaction (Fig. 3B). Leu418 and Leu421 in H10 are oriented towards the centre of the ERRγ-LBD and are conserved among almost all the NRs. In addition, almost all NRs conserve Leu399 in H9, and this Leu399 together with Leu418 and Leu421 in H10 take part in forming a hydrophobic core, which probably plays an intrinsic role in structural construction for homodimerization (Fig. 3C).

Binding Site of Bisphenol A—The binding site of BPA is constructed by a series of amino acid residues.

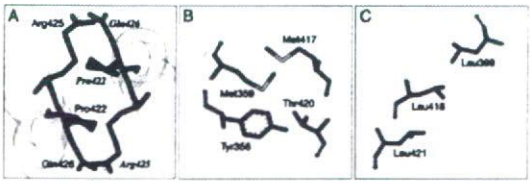

Fig. 3. **Intermolecular and intramolecular interactions of ERRγ-LBD.** (A) Dimer interface between H10 (blue) and *H10 (in the second molecule shown in italics)* is formed for amino acid residues such as Pro422–*Pro422*, Arg425–*Gln426*, and Gln426–*Arg425*. (B) Intramolecuar interaction between H7 (magenta) and H10 (blue) is seen for Tyr356 and Thr420, and for Met359 and Met417. (C) Highly conserved amino acid residues, Leu399 in H9, Leu418 and Leu421 in H10, are constructing a hydrophobic core.

Those in a range of 5 Å include Leu268, Cys269, Leu271, Ala272, Glu275 from H3; Trp305, Met306, Leu309, Val313, Arg316 from H5; Tyr326 from β-strand 1 (S1); Leu342, Leu345, Asn346, Ile349 from H7; Phe435 from H11 and Phe450 from H12 (Fig. 4A). In the BPA molecule, the two C_6H_4–OH (phenol) groups bind to the sp^3 carbon atom (sp^3-C) together with the two CH_3 groups, and thus their benzene-carbons adjacent to sp^3-C are arranged at the vertexes in a regular tetrahedron (Fig. 4B). It should be noted that BPA in the ERRγ-LBD complex is superimposed almost completely with BPA in the minimum-energy conformation (Fig. 4B). This demonstrates that BPA is present in the ERRγ-LBD binding pocket without any steric hindrance. Thus, BPA's phenol-hydroxyl oxygen atoms, C_6H_4–**O**H, are placed with a bond angle (O–sp^3–C–O) of about 105°, and are arranged to cross-link between Glu275/Arg316 and Asn346.

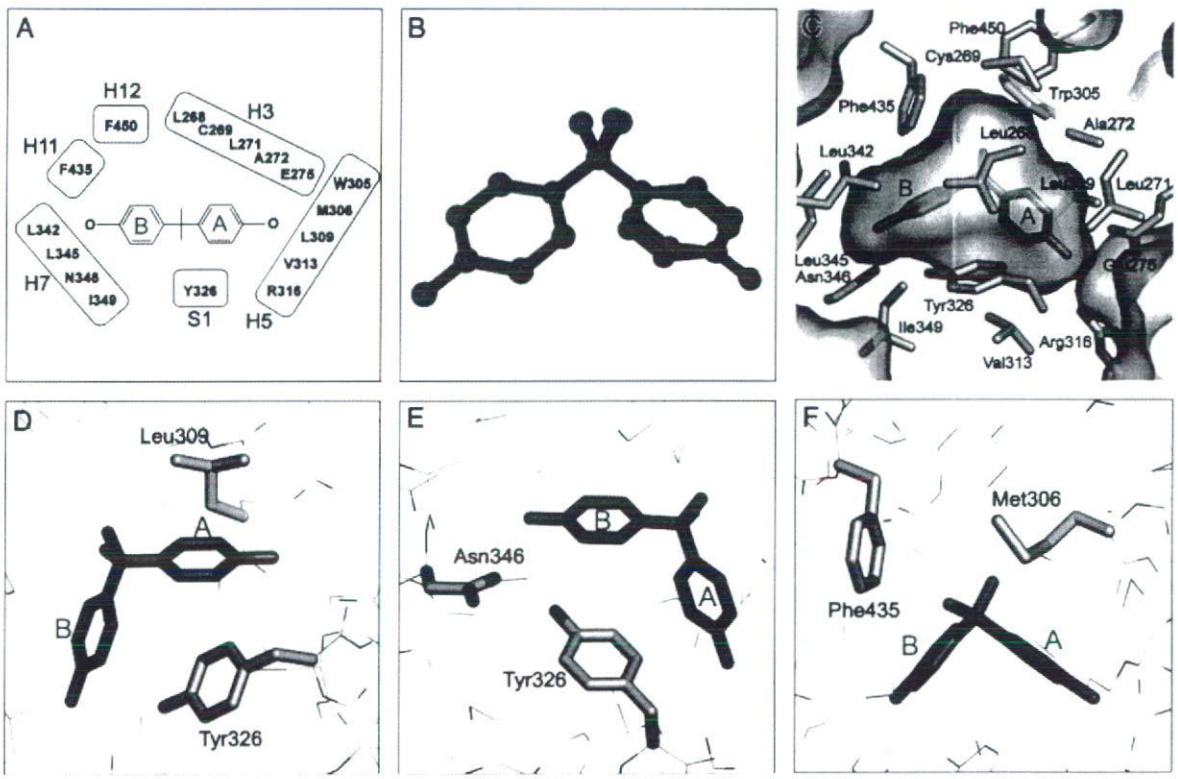

Fig. 4. **Identification of the binding sites of BPA in ERRγ-LBD.** (A) Schematic line-up of amino acid residues that form the LBP in ERRγ. The residues shown are in close proximity to BPA within 5 Å. (B) Superimposition of BPA (magenta) in the ERRγ-LBD complex and BPA (green) in the minimum-energy conformation calculated. They are almost completely overlaid, indicating that BPA fits the binding pocket of ERRγ-LBD without any conformational constrictions. The minimum-energy conformation was calculated and depicted by the conventional Hartree–Fock method using the computer program Gaussian (v. 03). (C) View of BPA in the cavity of ERRγ-LBD. The hydroxy groups of BPA's phenol-A and phenol-B rings are arranged to cross-link between Glu275/Arg316 and Asn346, respectively. (D) The BPA's A-ring is sandwiched with Leu309 and Tyr326 by characteristic hydrophobic interactions. The π face of A-ring interacts with the Leu309 isobutyl-methyl group, and the opposite π face of the same A-ring makes the T-shaped π/π interaction with Tyr326's phenol-benzene ring. (E) The BPA's B-ring is in a hydrogen bond with the Tyr326-phenol hydroxyl group. This OH/π bond appears to be a strong diving force to tether BPA in the ERRγ-LBP, together with the hydrogen bond between B-ring's hydroxy group and Asn346-β-carbonyl. (F) One of the CH_3 groups on the BPA's sp^3-C atom faces to Phe435 (H11) in a distance of 3.7 Å and another CH_3 group faces to the Met306 sulphur atom in a distance of 3.6 Å.

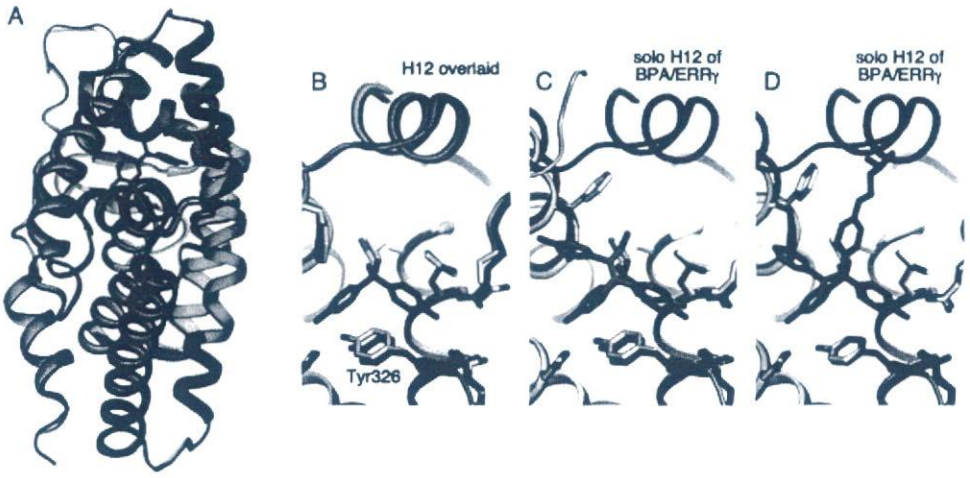

Fig. 5. **Superimposition of BPA or ERRγ-LBD and other ERRγ-LBD complexes.** (A) Superimposition of the whole LBD of BPA/ERRγ-LBD complex (blue) and the ERRγ-LBD apo form (grey) (1TFC; PDB code) (23). (B) The LBP of superimposed BPA/ERRγ-LBD complex (blue) and the ERRγ-LBD apo form (grey) (1TFC). The Tyr326-phenol groups are in a shift of about 10°, Tyr326-phenol of the BPA complex being underneath that of the apo form. (C) Superimposition of BPA/ERRγ-LBD complex (blue) and the DES/ERRγ-LBD complex (yellow) (1S9P) (23). The Tyr326-phenol groups are also in a slight shift. (D) Superimposition of the BPA/ERRγ-LBD complex (blue) and the 4-OHT/ERRγ-LBD (light blue) (1S9Q) (23). Superimposition of BPA (red) with DES (green) or 4-OHT (cyan) is carried out for α-helices to be overlaid. H12 in the BPA/ERRγ-LBD complex are shown in purple in all figures. H12 in the DES/ERRγ-LBD complex and in the 4-OHT/ERRγ-LBD complex are widely separated from a position in the activation conformation, and thus those are out of superimpositions between the BPA/ERRγ-LBD and the DES/ERRγ-LBD and 4–OHT/ERRγ-LBD complexes (C and D, respectively).

One of the two phenol-hydroxyl groups of BPA is anchored by hydrogen bonds with Glu275 (H3) and Arg316 (H5) at the one side of the ligand-binding pocket (LBP), while another hydroxyl group makes a hydrogen bond with Asn346 in H7 at the other side (Fig. 4C). Thus, BPA cross-links the residues Glu275/Arg316 and Asn346 with three hydrogen bonds. This is in stark contrast to the fact that diethylstilbestrol (DES) cross-links Glu275/Arg316 and His434 in H11 on the other side of the cavity (*23*). BPA's phenol-hydroxyl groups are not far enough apart to bridge between these Glu275/Arg316 and His434.

Key Amino Acid Tyr326 for Binding of Bisphenol A—Asn346 (H7) has been reported to interact with Tyr326 in S1 through a hydrogen bond (*23*, *24*). This hydrogen bond is also maintained in the BPA/ERRγ-LBD complex. In particular, we found that Tyr326 in the complex becomes the chief amino acid residue for BPA to be placed in the ERRγ-LBP, providing an appropriate and fitting space to pack BPA, having two phenol groups and two methyl groups. More importantly, Tyr326 interacts directly with BPA. The phenol group of the Tyr326 side chain keeps BPA's phenol-benzene rings A and B in the pocket by two strong interactions; i.e. by the hydrophobic *edge*-to-*face*-type, or T-shaped π/π interaction with BPA's benzene ring A, and by the OH/π interaction with BPA's benzene ring B (Fig. 4D and E). The Tyr-phenol benzene ring is able to make T-shaped π/π interactions with the aromatic side chains of amino acids such as Phe, Tyr, His and Trp (*25*, *26*). When one of six edges or vertexes of the benzene ring directs towards the π face of the counterpart aromatic ring, it makes so-called T-shaped π/π interaction(s). As seen in Fig. 4D, Tyr326's benzene ring indeed make a T-shaped π/π interaction with BPA's benzene ring A.

It should be noted that, at another π face on the opposite side, BPA's A ring interacts further with the Leu309 isobutyl-methyl groups (Fig. 4D). This interaction is also classified as a CH/π-type hydrophobic interaction. Consequently, there is a fascinating formation of sandwiched hydrophobic interactions of the A ring with Leu309 and Tyr326 (Fig. 4D). This is definitely a powerful driving force holding BPA in the LBD of ERRγ.

The Tyr326-phenol hydroxyl group makes another important interaction with BPA's benzene ring B. As shown in Fig. 4E, these are an OH/π interaction (*27*, *28*). OH/π interactions are one of the strongest interactions between amino acid side-chains (*25*, *26*). As a result, BPA's phenol B is tethered in the ERRγ-LBP complex by two essential interactions, the hydrogen bond with Asn346 and the OH/π bond with Tyr326.

It is noteworthy that Tyr326 has multiple interactions with BPA. In fact, Tyr326 might be in an ideal position to accept BPA in the ERRγ-LBP complex. When superimposition between ERRγ-LBD from the BPA/ERRγ-LBD complex and the ERRγ-LBD apo form (PDB code 1TFC) (*23*, *24*) was carefully checked, significant deviation was found for the Tyr326-phenol group (Fig. 5A and B). As shown in Fig. 5B, the Tyr326-phenol group in the BPA/ERRγ-LBD complex is pulled towards Asn346, shifting it through an angle of approximately 10°. This deviation keeps Tyr326-phenol group in the range of still stronger hydrogen bonds with Asn346, at a distance of 2.7 Å. All other amino acid residues in LBD are in exact agreement. In particular, the inside of the pocket is totally compatible with that of the apo form (Fig. 5A).

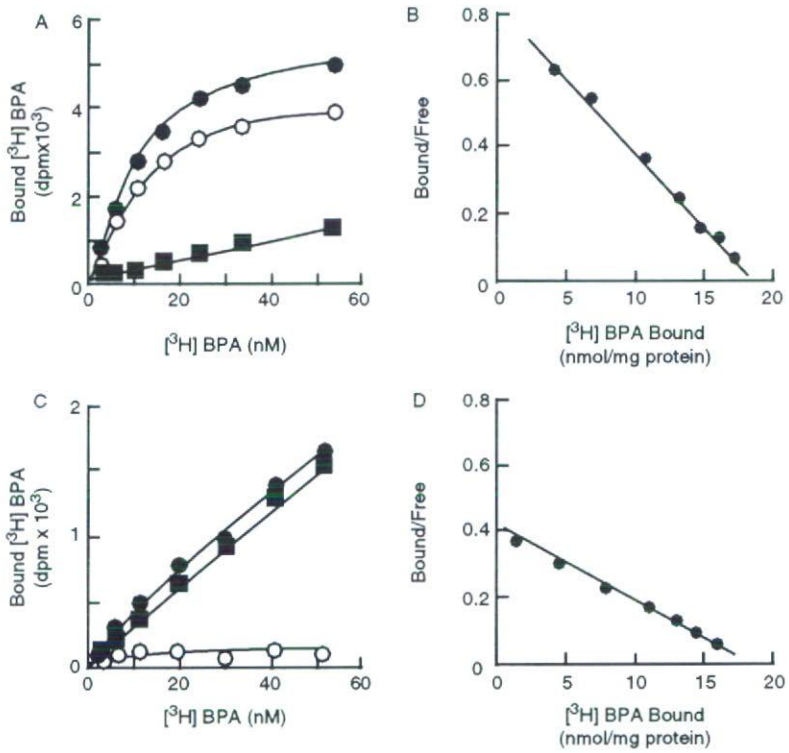

Fig. 6. **Receptor binding assays using tritium-labelled BPA.** (A) A sufficient specific binding of [^{3}H]BPA obtained in the saturation binding assay for wild-type ERRγ-LBD receptor. Closed circle, total binding; closed square, non-specific binding; and open circle, specific binding. (B) Scatchard plot analysis of [^{3}H]BPA for wild-type ERRγ-LBD. $K_D = 5.54 \pm 0.31$ nM, $B_{max} = 18.2 \pm 0.3$ nmol/mg protein. (C) No specific binding of [^{3}H]BPA shown in the saturation binding assay for ERRγ-LBD mutant receptor with E275A and R316A simultaneous substitutions. (D) Scatchard plot analysis of [^{3}H]BPA for ERRγ-LBD mutant receptor with N346A substitution. $K_D = 9.51 \pm 0.22$ nM, $B_{max} = 18.5 \pm 0.3$ nmol/mg protein. The Asn→Ala replacement was found to reduce approximately twice the dissociation constant, indicating that the Asn residue is important to the receptor binding of BPA presumably by the hydrogen-bonding between ERRγ-Asn-βCONH$_2$ and the BPA's phenol-hydroxyl group.

Interaction of Methyl Groups in Bisphenol A—BPA also has two methyl groups on the sp^3-C atom. One of these faces Phe435 (H11), and indeed the BPA-CH_3 and Phe435-phenyl groups are in close proximity (3.7 Å) to each other (Fig. 4F). On the other hand, another BPA-CH_3 group faces the Met306 sulphur atom with a non-covalent electron pair (3.6 Å between BPA-$\underline{C}H_3$ and Met306-$\underline{S}$) (Fig. 4F) making a form of electrostatic interaction. These interactions have been demonstrated by the drastically decreased binding activity that occurs in hexafluoro-BPA (designated as bisphenol AF), HO–C_6H_4–$C(CF_3)_2$–C_6H_4–OH, in which both CH_3 groups in BPA are replaced with trifluoromethyl CF_3 group. Electron-rich CF_3 would repel the electron-rich Phe-phenyl group and the Met-sulphur atom.

As mentioned earlier, BPA in the ERRγ-LBD complex is superimposed almost completely with BPA in the minimum-energy conformation (Fig. 4B). This implies that BPA fits spontaneously to the binding pocket of ERRγ-LBD without any conformational constraints, and binds specifically to each attachment position. It is likely that ERRγ possesses a binding pocket specifically adapted to the space requirements of the naturally occurring BPA-like ligand.

Superimposition of Bisphenol A/ERRγ-LBD Complex with Other Complexes—Superimposition of BPA and DES (1S9P) (*23*) in the ERRγ-LBD complexes shows conformational differences that can readily account for the differences in binding modes to the binding pocket. The phenol A ring of BPA superimposes almost completely with the corresponding A ring of DES, whereas the B rings orient in completely different directions (Fig. 5C). As a result, the phenol B ring of BPA heads towards H7 to capture Asn346 by its hydrogen bond, while that of DES goes towards H11 to restrain His434 also by a hydrogen bond.

Superimposition of the BPA complex and the 4-OHT complex (1S9Q) (*23*) of ERRγ-LBD, on the other hand, shows structural differences that make clear the difference in their activity mediated through the ERRγ. As before, the phenol A ring of BPA superimposes almost completely with the corresponding A ring of 4-OHT (Fig. 5D). Incontrast, the aromatic B ring of 4-OHT goes towards H11 with no hydrogen bond. The aromatic C ring of 4-OHT directs itself towards H12.

Greschik *et al.* (*23*) have reported that the binding of DES and 4-OHT to ERRγ-LBD dissociates the H12 region from the LBD body. DES- and 4-OHT-mediated

activities were explained by the three-dimensional structure of the DES/or 4-OHT/ERRγ-LBD complex, in which helix 12 is widely separated from a position in the activation conformation. Indeed, their H12s are out of superimpositions between the BPA/ERRγ-LBD and the DES/ or 4–OHT/ERRγ-LBD complexes (Fig. 5C and D). This repositioning of H12 by DES and 4-OHT deactivates ERRγ, because the receptor becomes unable to recruit coactivator proteins at the appropriate position. The LBD structure of ERRγ apo form has also been solved (*23*, *24*), and as expected from its very high constitutive activity, H12 of this non-liganded ERRγ-LBD is folded in the activation conformation (Fig. 5A).

Bisphenol A Holds ERRγ-LBD in the Activation Conformation—One of the most important findings in the present study is that H12 in the BPA/ERRγ-LBD complex is in the transcriptionally active conformation. H12 is associated firmly with the LBD body, where the coactivator binds. When we compared this crystal structure with the reported crystal structure (1TFC) of the apo form of ERRγ-LBD (*23*), almost no conformational changes were shown for almost all the atoms including both the main and side chains from H1 to H12 (Fig. 5A). Superimposition of the ERRγ-LBD from the BPA/ERRγ-LBD complex and the apo ERRγ-LBD shows their exact and entire agreement. In particular, the positioning and conformation of H12 is totally compatible with that of the apo form (Fig. 5A and B). Although H12's activation conformation in the apo form appeared to be maintained by the presence of a peptide derived from the coactivator protein SRC-1, H12 in the BPA/ERRγ-LBD complex is in fact in the activation conformation without the SRC-1 peptide.

These conformational consequences verify the high functional activity of BPA. ERRγ *per se* elicits a very high basal activity in the luciferase reporter gene assay. BPA was found to maintain this high spontaneous constitutive activity in ERRγ for a range of concentrations from 10^{-10} to 10^{-5} M BPA (*10*). Furthermore, BPA reverses the deactivation activity of 4-OHT, indicating that BPA displaces 4-OHT and repositions the H12 from the transcriptionally inactive conformation to the active conformation. It should be noted that the compounds that deactivate the receptor are termed as 'inverse agonist,' whereas those that inhibit such inverse agonists are defined as 'inverse antagonist.' Thus, BPA indeed acts as an inverse antagonist against the inverse agonist 4-OHT in ERRγ.

Structural Demonstration of the Binding Sites by Site-directed Mutagenesis—The amino acid residues in the BPA-binding site of ERRγ-LBD were substituted with Ala by means of the site-directed mutagenesis. Those included Glu275, Met306, Leu309, Arg316, Tyr326, Asn346 and Phe435 in the binding pocket. The resulting mutant receptors were examined by the saturation binding assay using tritium-labelled BPA (Fig. 6A and B). When Glu275 and Arg316 were substituted simultaneously, the mutant receptor exhibited almost no specific binding (Fig. 6C), indicating that these residues are critically important to bind BPA to the pocket. In contrast, [^{3}H]BPA was found to bind to Asn346Ala mutant receptor (B_{max} = 18.5 nmol/mg) as well as wild-type receptor (18.2 nmol/mg), although its binding affinity for the mutant was approximately 2-fold weaker (K_D = 9.51 nM) than that for the wild-type (5.54 nM) (Fig. 6D). All other mutant receptors exhibited considerably reduced specific binding and drastically weakened binding ability (10–20-fold larger K_D values). The results clearly evidenced that the structural elements complementary to BPA are indeed its binding sites.

Conclusion and Perspectives—The present study clearly indicates that the nuclear receptor ERRγ possesses a space in its LBD to which BPA can bind highly specifically and selectively. It is still not clear whether, under physiological conditions, ERRγ can function without an endogenous ligand, nor what ERRγ's physiological functions may be. The results we present imply that ERRγ may in fact have a BPA-like endogenous ligand, and will facilitate the design of novel specific agonist and antagonist compounds.

The binding affinity of [^{3}H]BPA to ERRγ-LBD is extremely high, with a K_D value of 5.5 nM. Thus, it is an immediate and important requirement to evaluate whether the previously reported effects of BPA at low doses are mediated through ERRγ and its specific target gene(s). At the same time, it is necessary to clarify what the physiological roles of ERRγ are, and to examine the extent of, and direction in which, BPA may influence these. This is particularly important because ERRγ is expressed in a tissue-restricted manner, for example, very strongly in the mammalian foetal brain and also in the placenta, at sites that could have important outcomes for the newborn.

We thank Prof. Ian A. Meinertzhagen, Dalhousie University, Canada, for reading the manuscript. This study was supported by Health and Labour Sciences Research Grants to Y.S., for Research on Risk of Chemical Substances, from the Ministry of Health, Labor and Welfare of Japan. This work was also supported in part by grants-in-aid from the Ministry of Education, Culture, Sports, Science and Technology of Japan to Y.S. We thank the staff of the SPring-8 BL38B1 beamline for help with the X-ray diffraction experiments. The work was supported by a grant for the National Project on Protein Structural and Functional Analyses from the Ministry of Education, Culture, Sports, Science and Technology of Japan. Atomic coordinates for the structure have been deposited in the Protein Data Bank with accession code 2E2R.

REFERENCES

1. Krishnan, A.V., Stathis, P., Permuth, S.F., Tokes, L., and Feldman, D. (1993) Bisphenol-A: an estrogenic substance is released from polycarbonate flasks during autoclaving. *Endocrinology* **132**, 2279–2286
2. Olea, N., Pulgar, R., Pérez, P., Olea-Serrano, F., Rivas, A., Novillo-Fertrell, A., Pedraza, V., Soto, A.M., and Sonnenschein, C. (1996) Estrogenicity of resin-based composites and sealants used in dentistry. *Environ. Health Perspect.* **104**, 298–305
3. Nagel, S.C., vom Saal, F.S., Thayer, K.A., Dhar, M.G., Boechler, M., and Welshons, W.V. (1997) Relative binding affinity-serum modified access (RBA-SMA) assay predicts the relative *in vivo* bioactivity of the xenoestrogens